

Tetra-Coordinated Organoboron Complexes with Triaminoguanidine-Salicylidene based Ligands: Aggregation Induced Enhanced Emission and Mechanoresponsive Features

Balamurugan Tharmalingam,^{#a,b} Rajendran Kishore Kumar,^{#a} Ottoor Anitha,^a Werner Kaminsky,^c Jan Grzegorz Malecki,^d Balasubramanian Murugesapandian^{a,*}

^aDepartment of Chemistry, Bharathiar University, Coimbatore, 641046, Tamil Nadu, India. E-mail: mpandian@gmail.com; bmurugesapandian@buc.edu.in Fax: +91-422-2422387; Tel: +91-422-2428312.

^bState Key Laboratory of Fine Chemicals, Frontier Science Center for Smart Materials, School of Chemical Engineering, Dalian University of Technology, Dalian 116024 (P. R. China)

^cDepartment of Chemistry, University of Washington, Seattle, WA 98195, USA.

^d Institute of Chemistry, University of Silesia, Szkolna 9, 40-006 Katowice, Poland

Equal contribution

Table of Contents

1	Table S1. Comparative table between previously reported organoboron AIE gen bearing ES IPT unit	S5, S6
2	Fig. S1. ¹ H NMR Spectrum of 6 in DMSO- <i>d</i> ₆ .	S7
3	Fig. S2. ¹³ C NMR Spectrum of 6 in DMSO- <i>d</i> ₆ .	S8
4	Fig. S3. ¹¹ B NMR Spectrum of 6 in DMSO- <i>d</i> ₆ .	S8
5	Fig. S4. The HRMS of compound 6 .	S9
6	Fig. S5. ¹ H NMR Spectrum of 7 in CDCl ₃ .	S10
7	Fig. S6. ¹³ C NMR Spectrum of 7 in DMSO- <i>d</i> ₆ .	S11
8	Fig. S7. ¹¹ B NMR Spectrum of 7 in CDCl ₃ .	S11
9	Fig. S8. The HRMS of compound 7 .	S12

10	Fig. S9. ^1H NMR Spectrum of 8 in $\text{DMSO-}d_6$	S13
11	Fig. S10. ^{13}C NMR Spectrum of 8 in $\text{DMSO-}d_6$.	S13
12	Fig. S11. ^{11}B NMR Spectrum of 8 in CDCl_3 .	S14
13	Fig. S12. The HRMS of compound 8 .	S15
14	Fig. S13. ^1H NMR Spectrum of 9 in $\text{DMSO-}d_6$.	S16
15	Fig. S14. ^{13}C NMR Spectrum of 9 in $\text{DMSO-}d_6$.	S16
16	Fig. S15 ^{11}B NMR Spectrum of 9 in CDCl_3 .	S17
17	Fig. S16. The HRMS of compound 9 .	S18
18	Fig. S17. ^1H NMR Spectrum of 10 in $\text{DMSO-}d_6$.	S19
19	Fig. S18. ^{13}C NMR Spectrum of 10 in $\text{DMSO-}d_6$.	S19
20	Fig. S19. ^{11}B NMR Spectrum of 10 in $\text{DMSO-}d_6$.	S20
21	Fig. S20. The HRMS of compound 10 .	S21
22	Fig. S21 Two-dimensional chain like supramolecular network of 6 .	S22
23	Fig. S22 Two-dimensional polymeric supramolecular network of 7 .	S22
24	Fig. S23 Two-dimensional polymeric supramolecular network of 8 .	S23
25	Fig. S24 Dimeric structure of compound 9 .	S23
26	Fig. S25 Two-dimensional supramolecular network of 9 .	S24
27	Fig. S26 Two-dimensional chain like supramolecular network of 10 .	S24
28	Fig. S27. Absorption spectra of boron compounds 6-10 (A - E) in various solvents	S25

	with different polarities at room temperature.	
29	Fig. S28. Enol form of selected frontier molecular orbital of organoboron complexes 6-10 based on optimized ground state geometry. Calculation was performed at B3LYP/6-31G(d) level with Gaussian 16.	S26
30	Fig. S29. Keto form of selected frontier molecular orbital of organoboron complexes 6-10 based on optimized ground state geometry. Calculation was performed at B3LYP/6-31G(d) level with Gaussian 16.	S26
31	Table S2. Selected bond lengths (Å) for [6-10] from X-ray and calculated structures using the B3LYP 6-31G method.	S27
32	Table S3. Electronic transition for organoboron complexes 6-10 calculated using the B3LYP 6-31G method.	S27
33	Table S4. UV-visible absorption and emission spectra of 6-10 in different solvents at room temperature.	S28
34	Fig. S30. (A) Emission spectra of 6 in different water fractions in THF and water mixture binary solvent; $\lambda_{\text{ex}} = 420$ nm. (B) Plots of emission intensity vs water fraction. (C) Fluorescent images in different water fractions (under UV light).	S29
35	Fig. S31. (A) Emission spectra of 7 in different water fractions in THF and water mixture binary solvent; $\lambda_{\text{ex}} = 420$ nm. (B) Plots of emission intensity vs water fraction. (C) Fluorescent images of in different water fractions (under UV light).	S30
36	Fig. S32. (A) Emission spectra of 8 in different water fractions in THF and water mixture binary solvent; $\lambda_{\text{ex}} = 420$ nm. (B) Plots of emission intensity vs water fraction. (C) Fluorescent images of in different water fractions (under UV light).	S31
37	Fig. S33. UV-visible absorption spectra of compounds 6-10 (A-E) in THF-H ₂ O (0-90 %) mixture with different water fractions.	S32
38	Fig. S34. DLS images of compounds (6-10) with particle size distribution in THF-H ₂ O mixture (A, B) 6 (60 & 90%), (C, D) 7 (70 & 90%), (E, F) 8 (50 & 70%), (G, H) 9 (70 & 90%) and (I, J) 10 (70 & 90%)	S33
39	Table S5. Results from DLS for the complex 6-10 .	S34

40	Fig. S35. Emission spectra of 6 -10 in THF-H ₂ O and THF-glycerol.	S34
41	Fig. S36. (A). Images of the boron compounds (7 & 8) under UV-lamp. (B) Solid state emission spectra of compounds (7 & 8) crystals and ground samples.	S35
42	Fig. S37. (A) Normalized spectrum of the compound 6 before and after grinding. (B) Normalized spectrum of the compound 9 before and after grinding. (C) Normalized spectrum of the compound 10 before and after grinding.	S36
43	Fig. S38. SEM images of compounds 9 &10 (A&B) before and (C&D) after grinding respectively.	S36
44	Table S6. Crystal parameters and structure refinement data for compound 6-10 .	S37, S38
45	References	S39

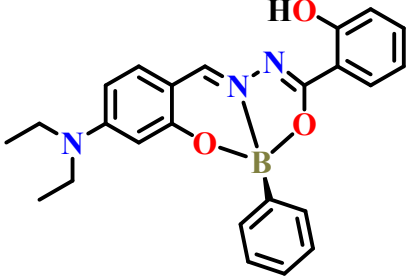
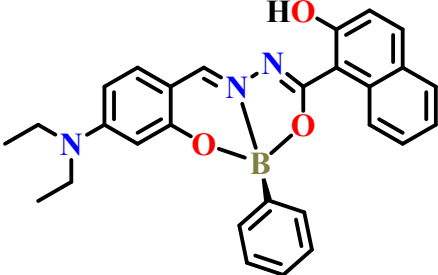
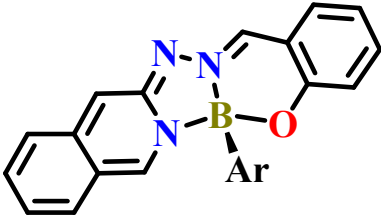
Stock solution preparation for spectroscopic measurements

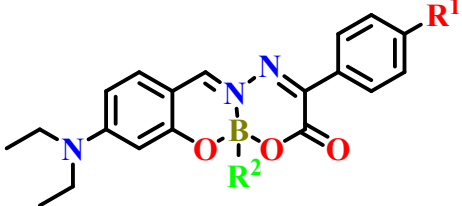
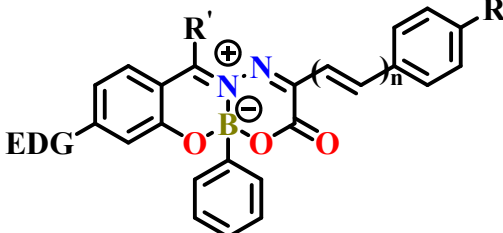
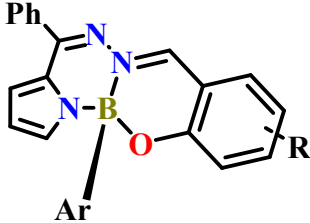
Stock solutions of 1×10^{-5} were prepared for the solvent effect studies of boron compounds 6-10. For aggregation studies, stock solutions of 1×10^{-4} were made using double-distilled ultrapure water and THF as solvents.

Computation Details

DFT calculations were performed by using the Gaussian 16 package.¹ The ground state geometries were optimized using DFT at the B3LYP/6-31G(d). The electronic excited state energies of the compounds were calculated by time-dependent DFT (TDDFT) with B3LYP functional and 6-31G(d) basis set based on the optimized ground state geometry.

Table S1. Comparative table between previously reported organoboron AIE gen bearing ES IPT unit

S.No.	Compound	AIE with ES IPT	Reference
1. (a)	 <p>DPDP</p>	AIE Only	2
1. (b)	 <p>DPDN</p>	AIE Only	
2.		AIE Only	3

3.	 <p>R^1 - H, CF_3, CN, NO_2 R^2-C_6H_5</p>	-	4
4.	 <p>$R' = H, Me, Et, iPr$ $R = H, CF_3$</p>	-	5
5.		AIE Only	6
6.	This work	AIE with ESIPT unit	

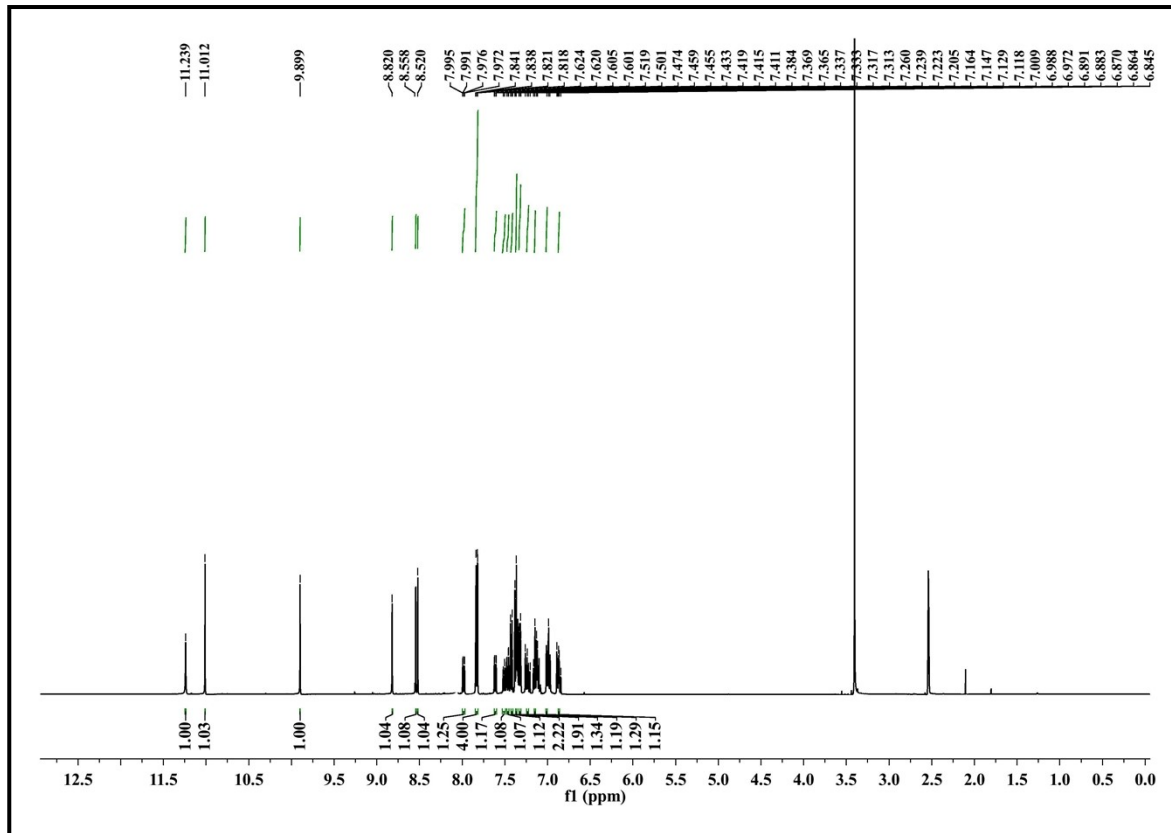


Fig. S1. ^1H NMR Spectrum of **6** in $\text{DMSO-}d_6$

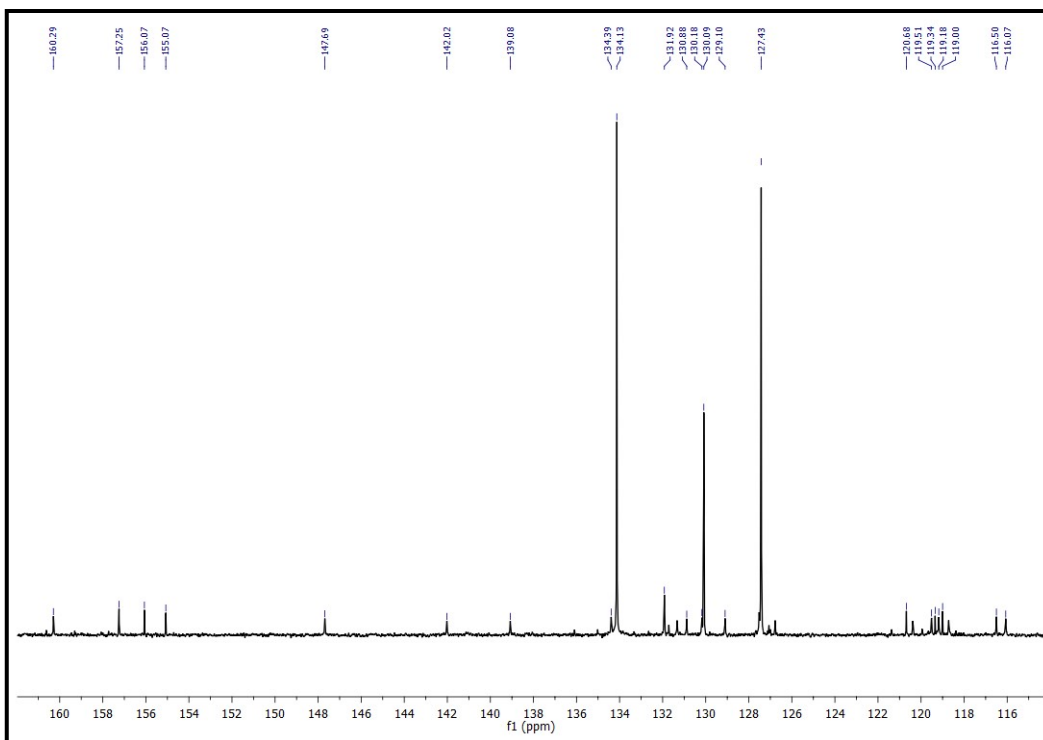


Fig. S2. ^{13}C NMR Spectrum of **6** in $\text{DMSO-}d_6$.

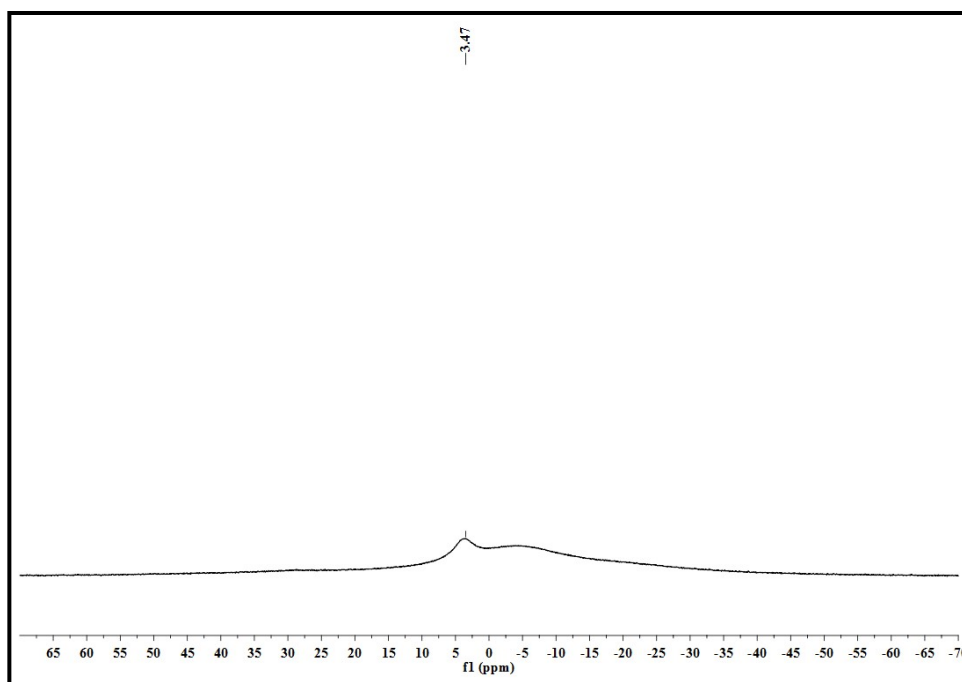


Fig. S3. ^{11}B NMR Spectrum of **6** in $\text{DMSO-}d_6$.

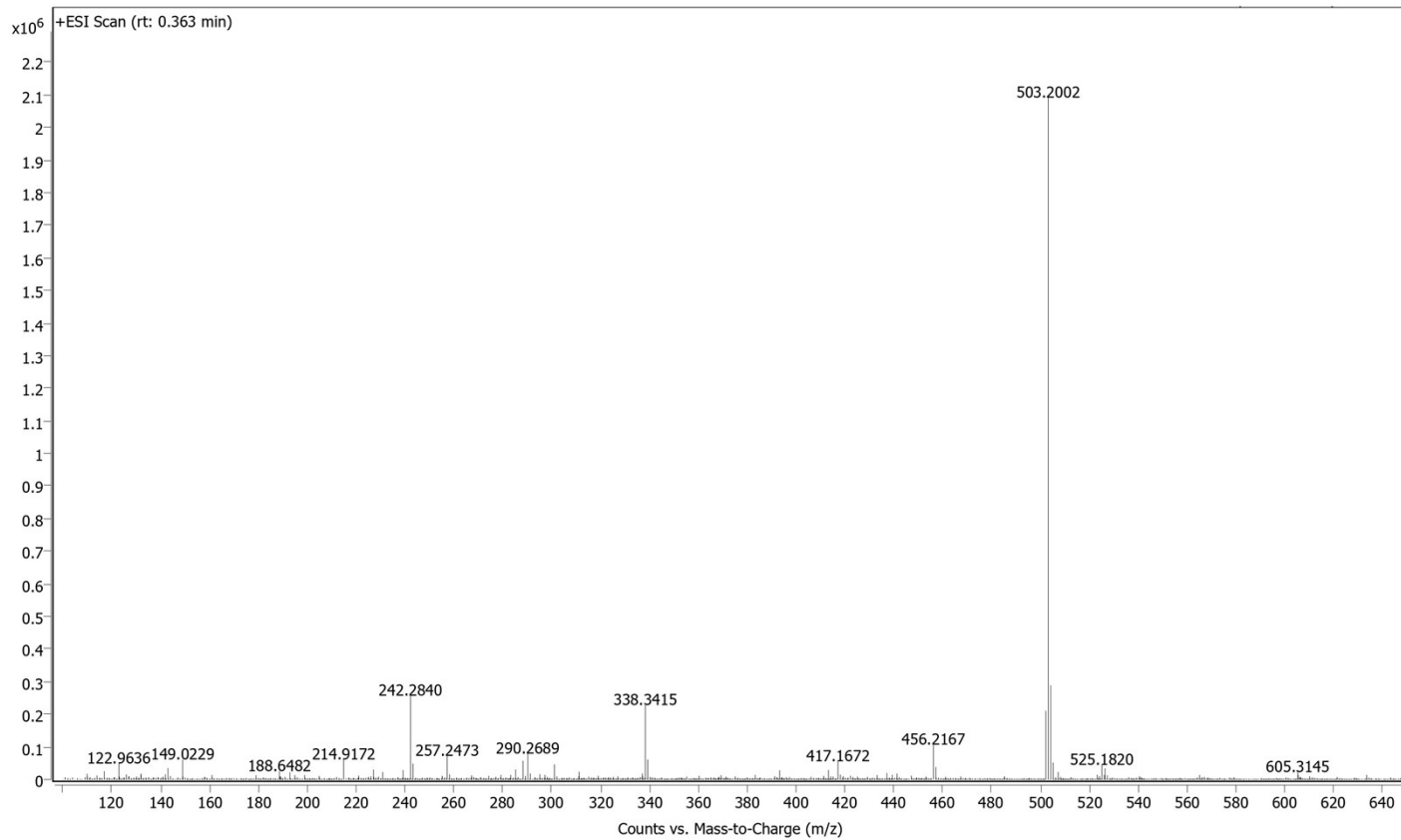


Fig. S4. The HRMS of compound 6.

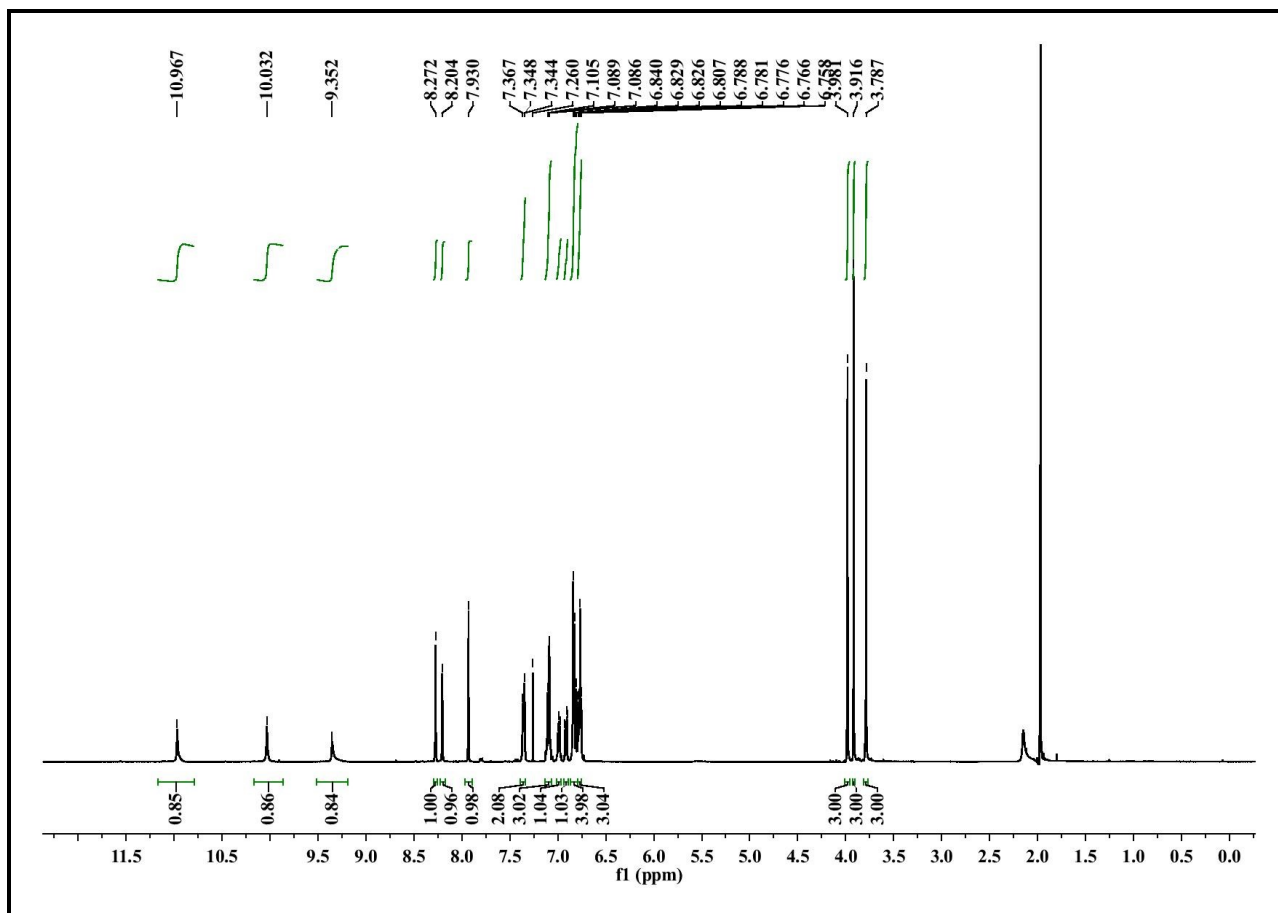


Fig. S5. ^1H NMR Spectrum of 7 in CDCl_3 .

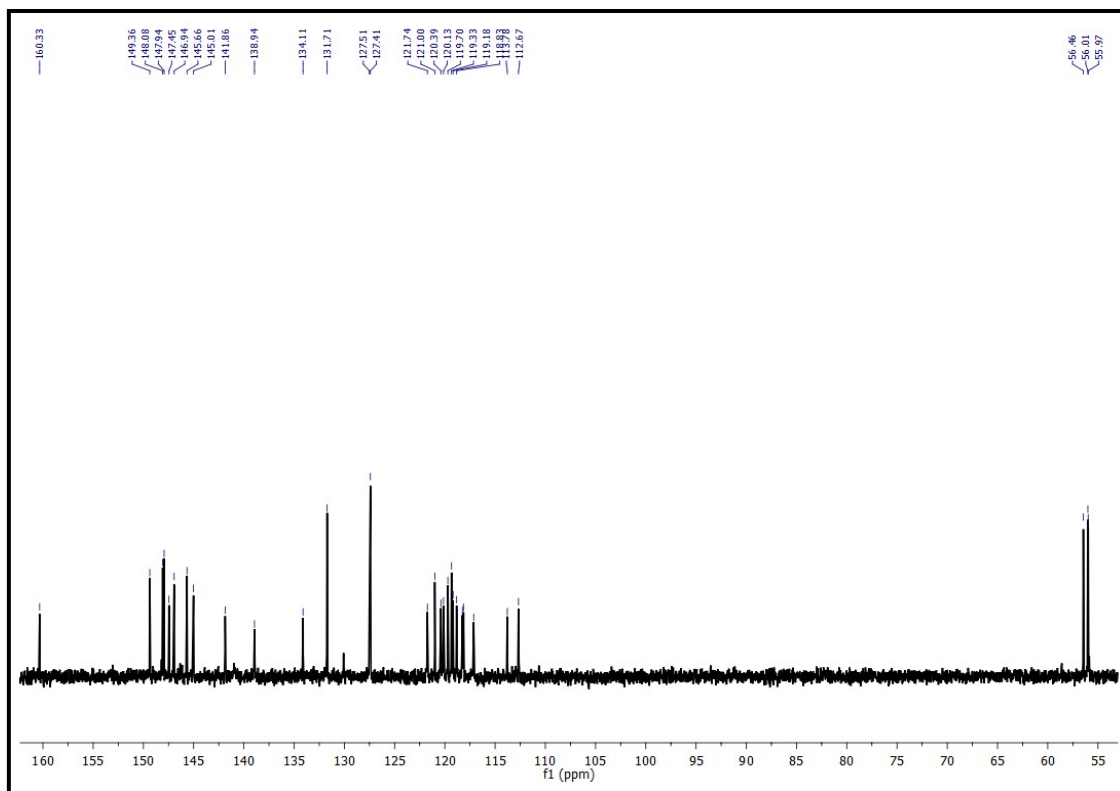


Fig. S6. ^{13}C NMR Spectrum of 7 in DMSO-d_6 .

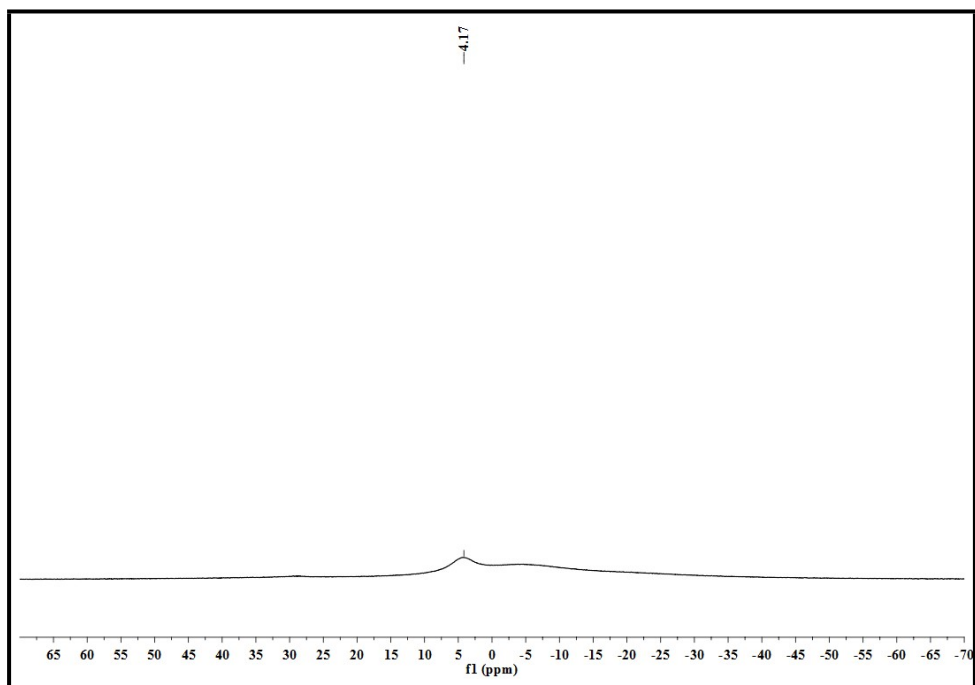


Fig. S7. ^{11}B NMR Spectrum of 7 in CDCl_3 .

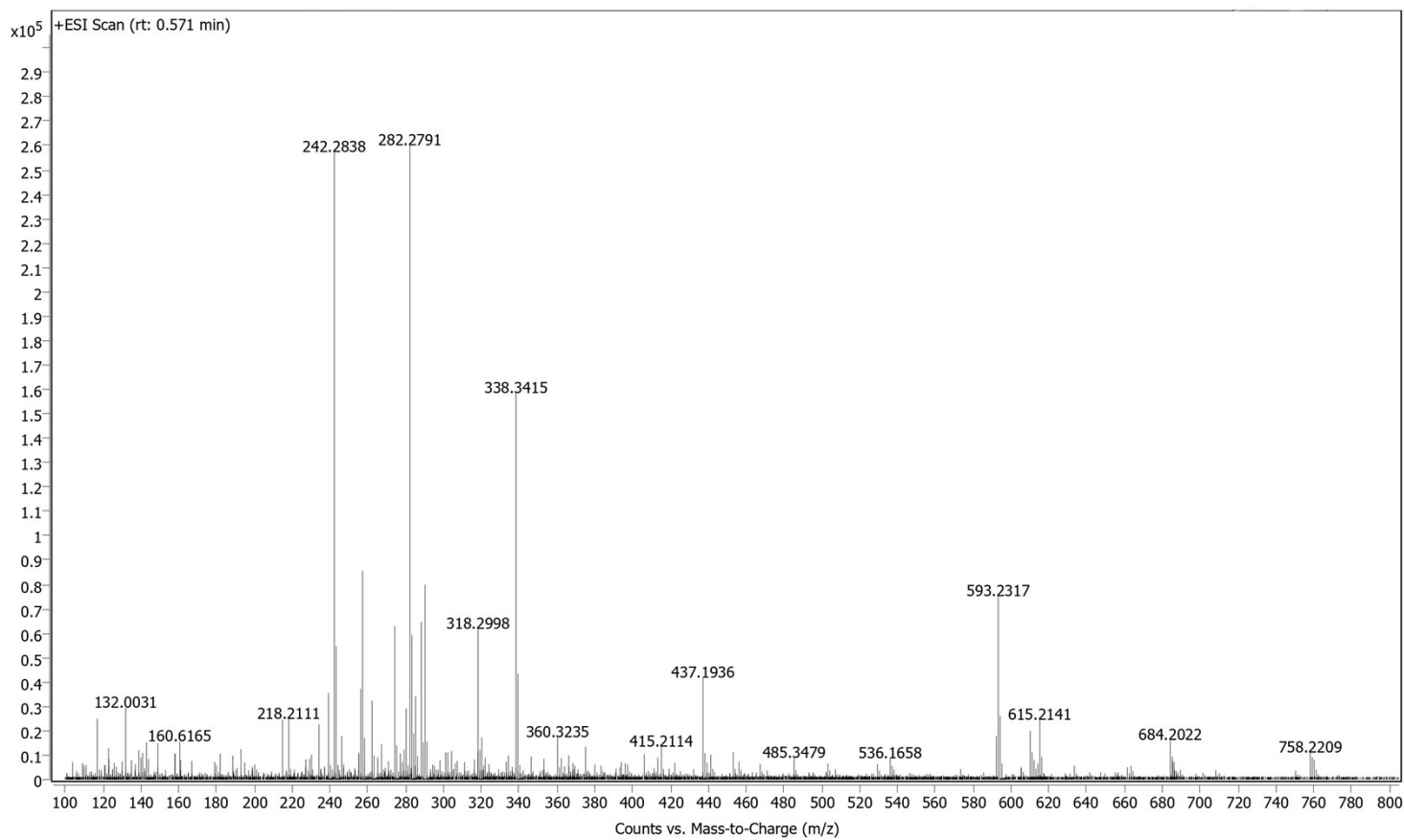


Fig. S8. The HRMS of compound 7.

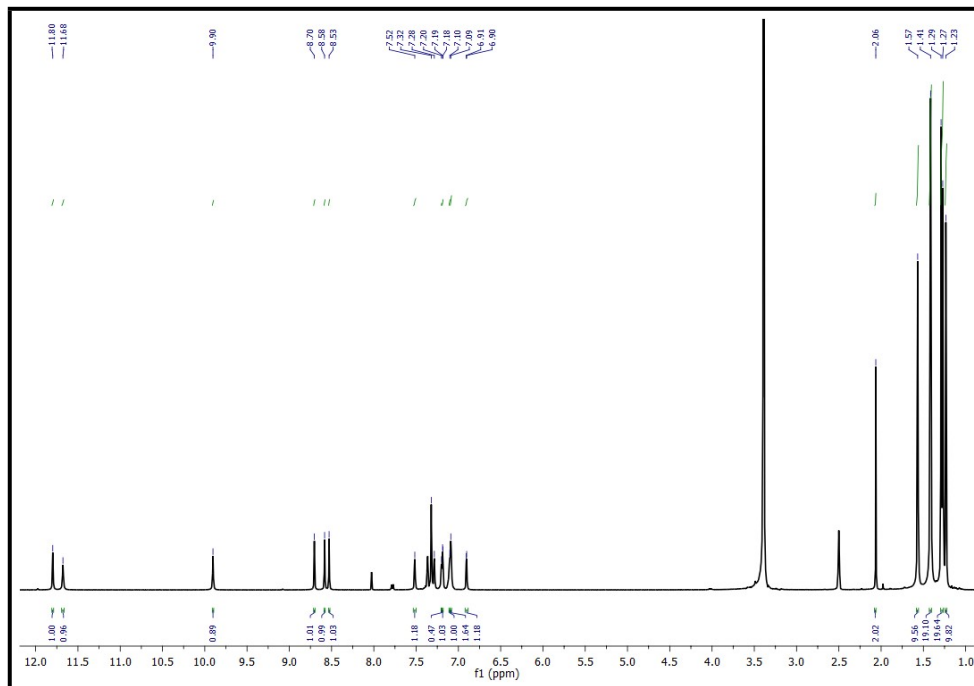


Fig. S9. ^1H NMR Spectrum of **8** in DMSO-d_6 .

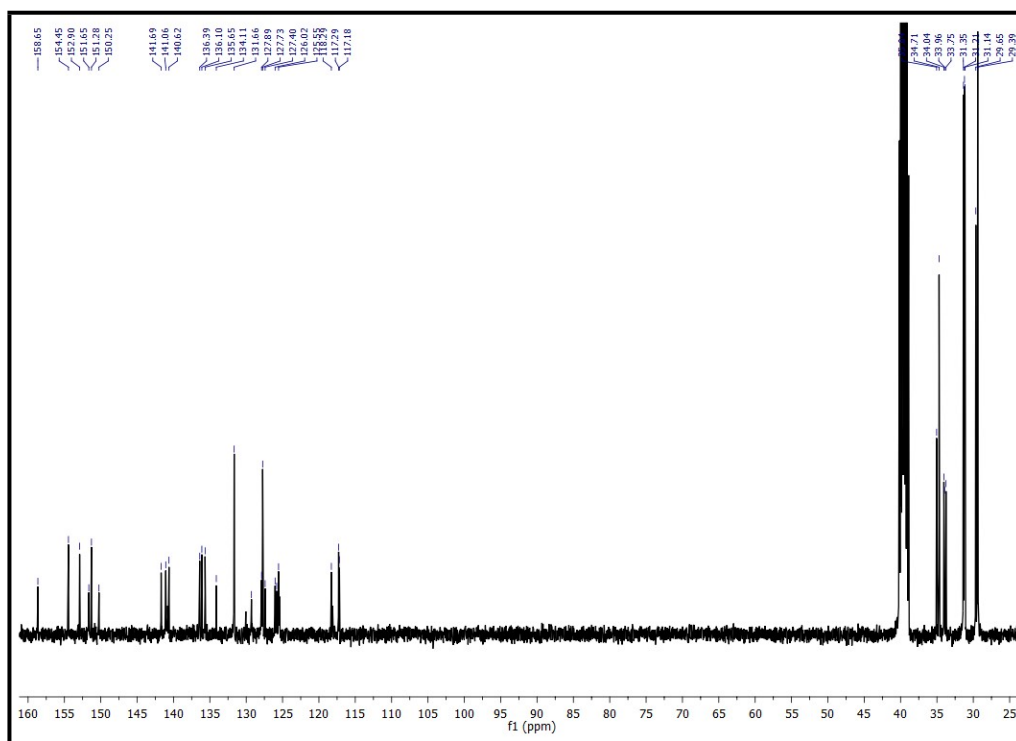


Fig. S10. ^{13}C NMR Spectrum of **8** in DMSO-d_6 .

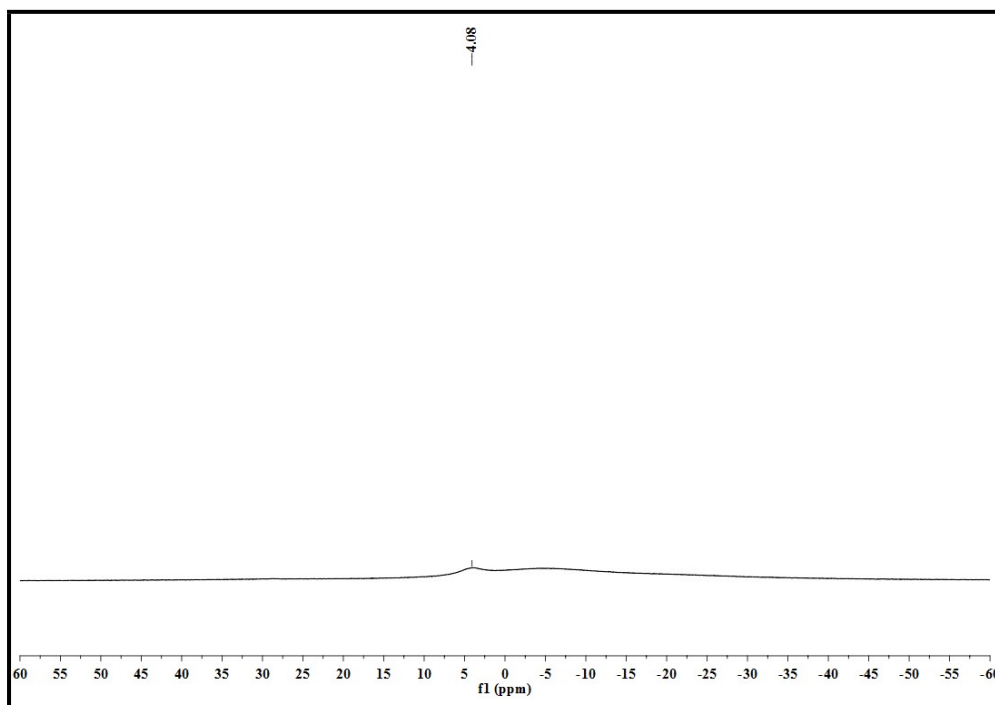


Fig. S11. ^{11}B NMR Spectrum of **8** in CDCl_3 .

LN-01 #83 RT: 0.84 AV: 1 NL: 1.39E7
T: FTMS + p ESI Full ms [150.0000-1000.0000]

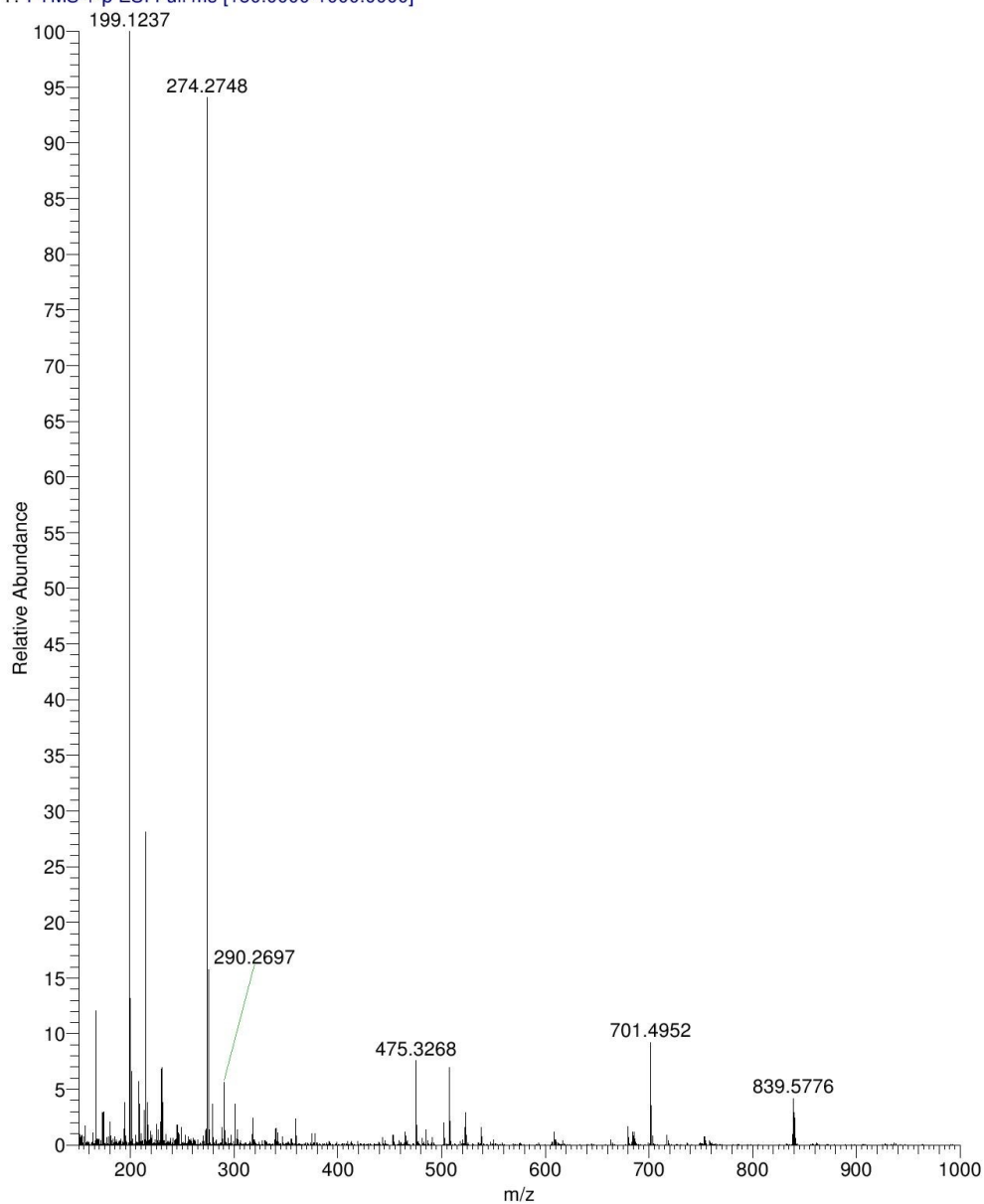


Fig. S12. The HRMS of compound 8.

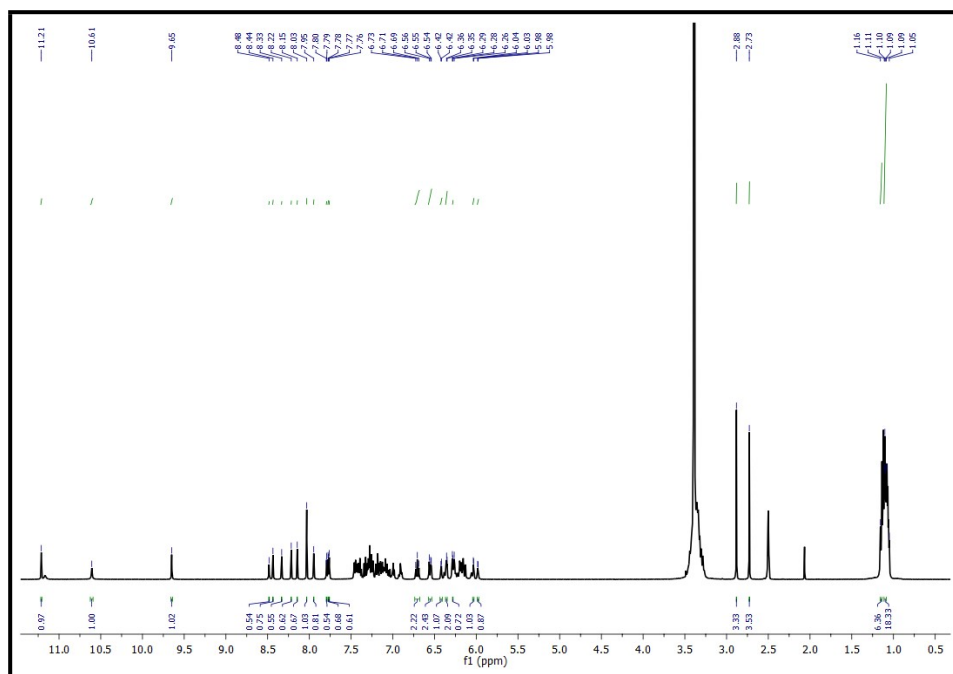


Fig. S13. ^1H NMR Spectrum of **9** in DMSO-d_6 .

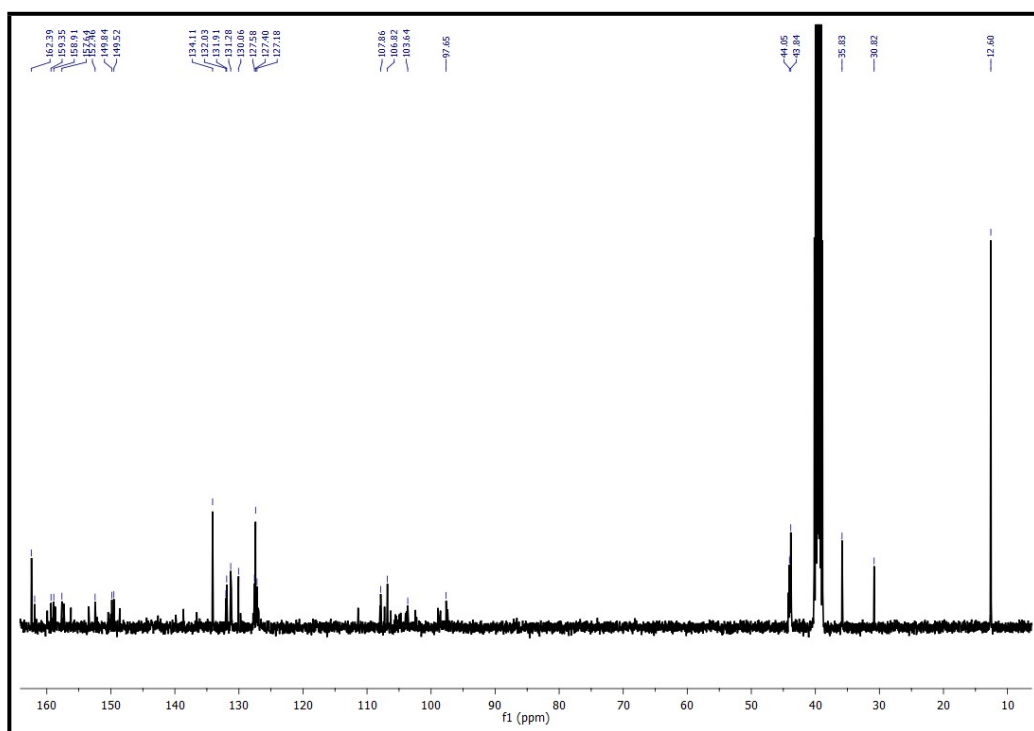


Fig. S14. ^{13}C NMR Spectrum of **9** in DMSO-d_6 .

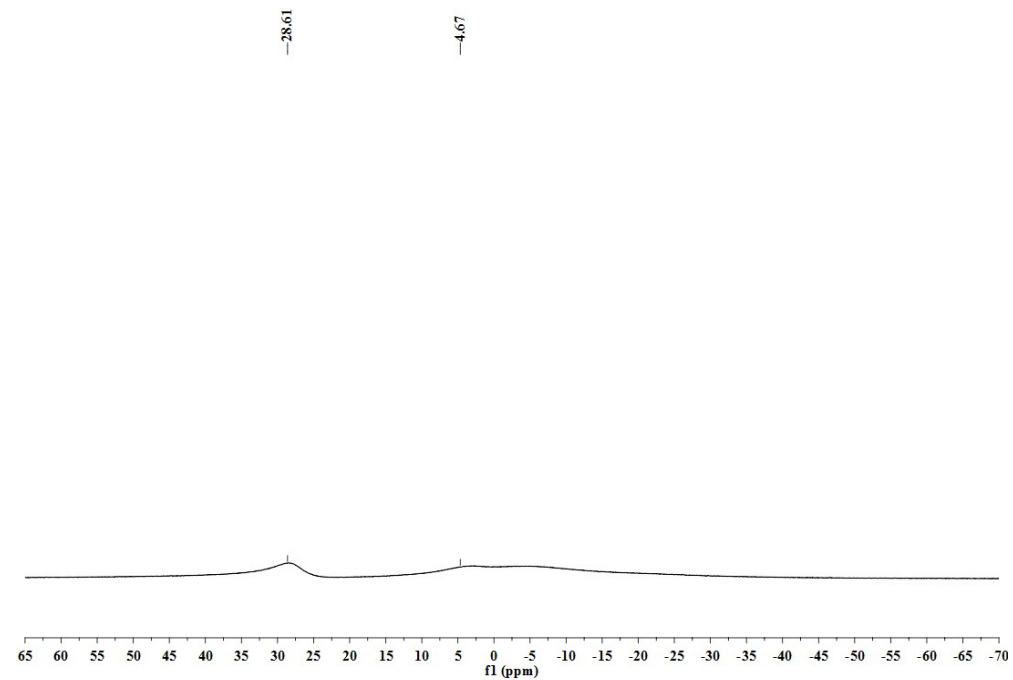


Fig. S15 ^{11}B NMR Spectrum of **9** in CDCl_3 .

LN-04 #45 RT: 0.46 AV: 1 NL: 4.62E8
T: FTMS + p ESI Full ms [150.0000-1000.0000]

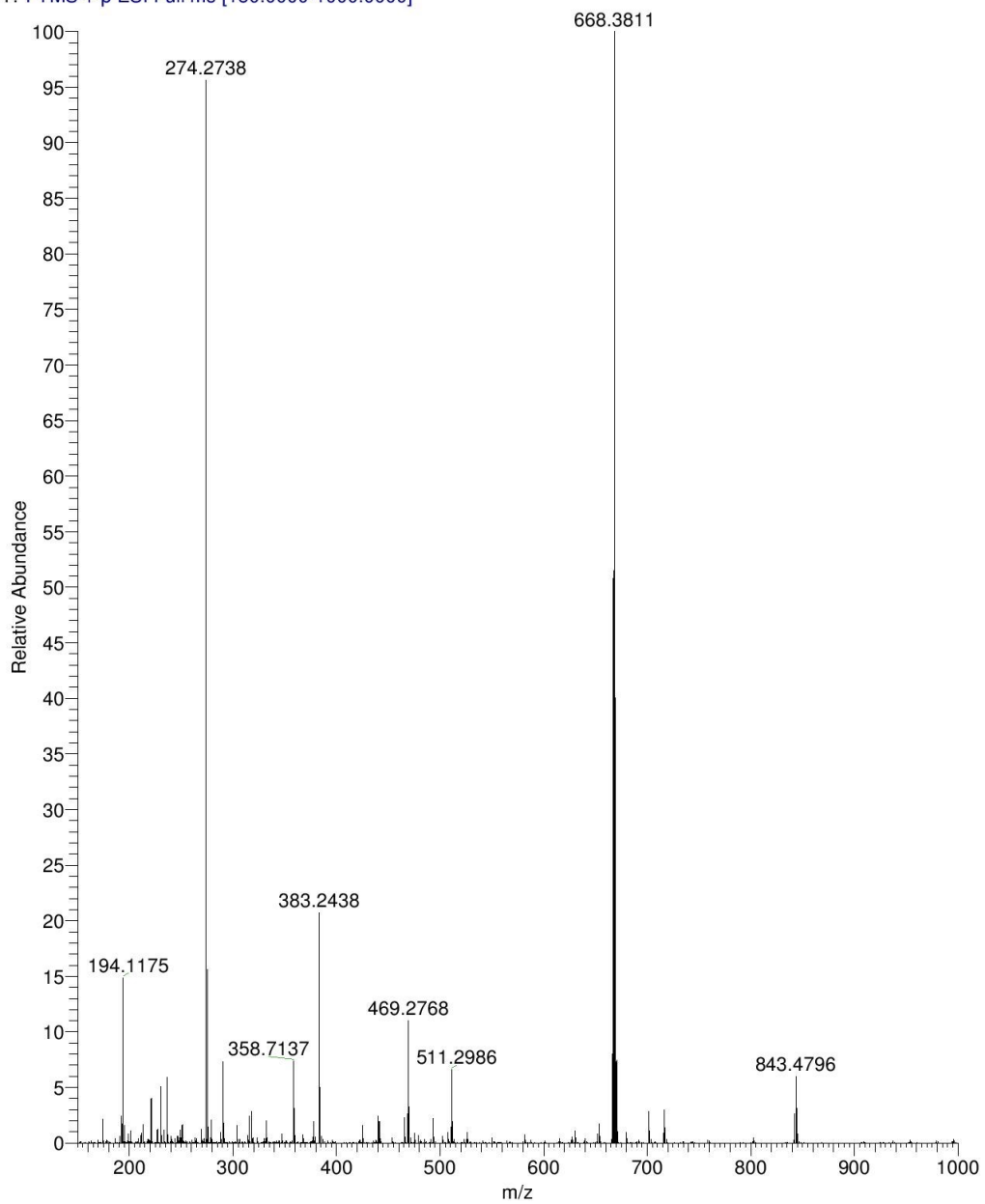


Fig. S16. The HRMS of compound **9**.

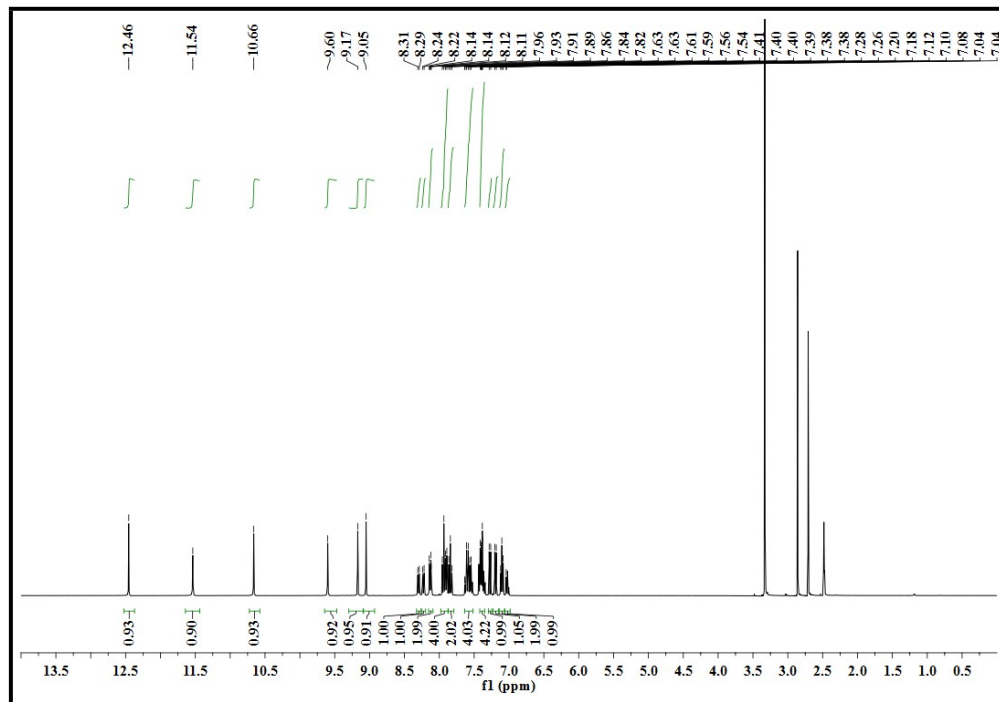


Fig. S17. ^1H NMR Spectrum of **10** in $\text{DMSO-}d_6$.

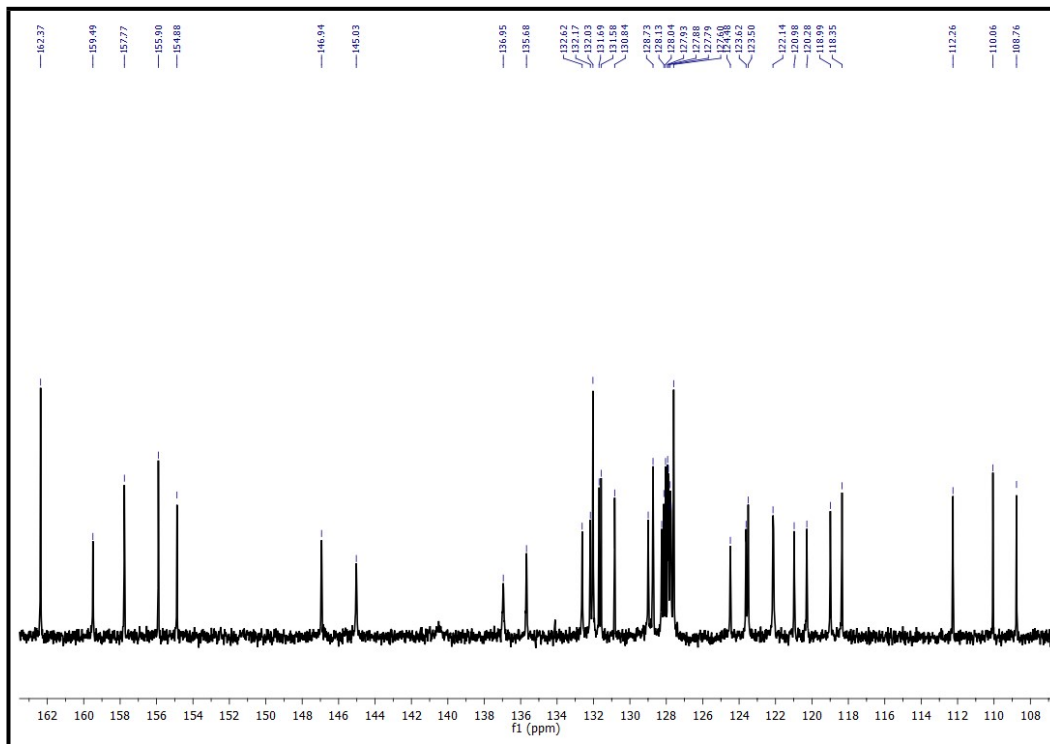


Fig. S18. ^{13}C NMR Spectrum of **10** in $\text{DMSO-}d_6$.

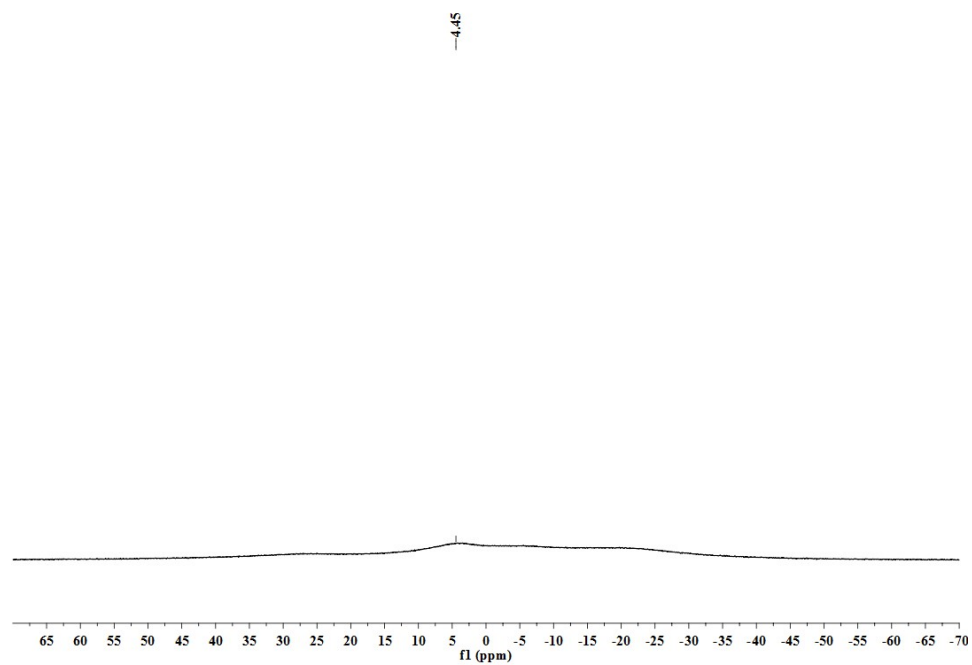


Fig. S19. ^{11}B NMR Spectrum of **10** in $\text{DMSO-}d_6$.

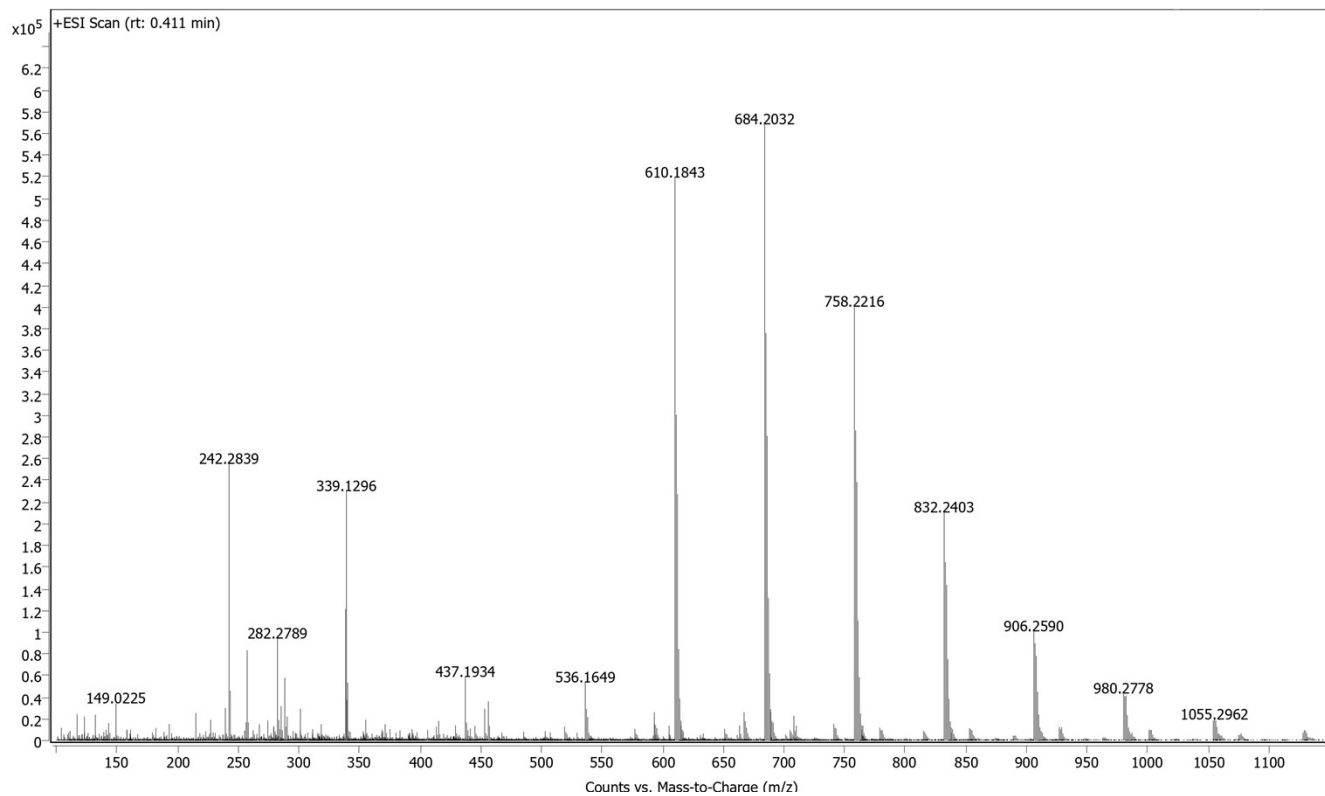


Fig. S20. The HRMS of compound 10.

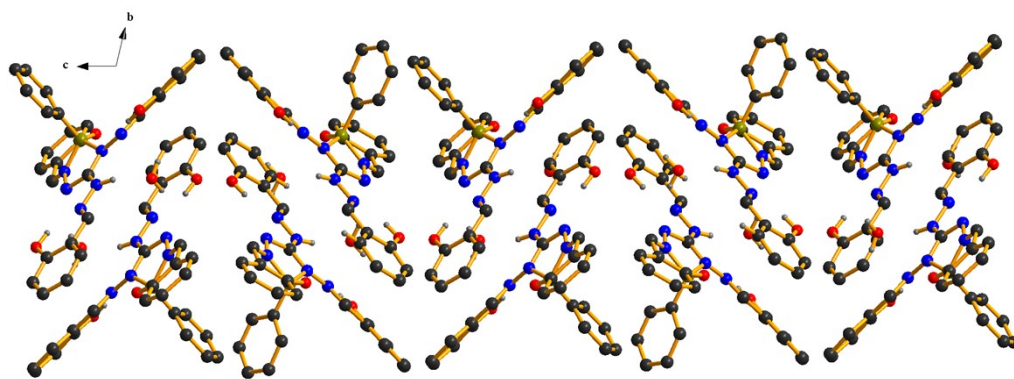


Fig. S21 Two-dimensional chain like supramolecular network of **6**.

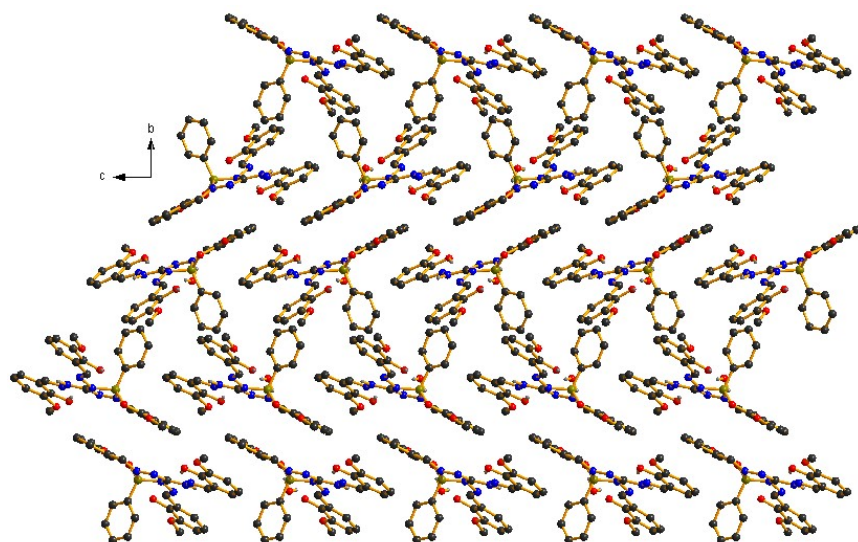


Fig. S22 Two-dimensional polymeric supramolecular network of **7**.

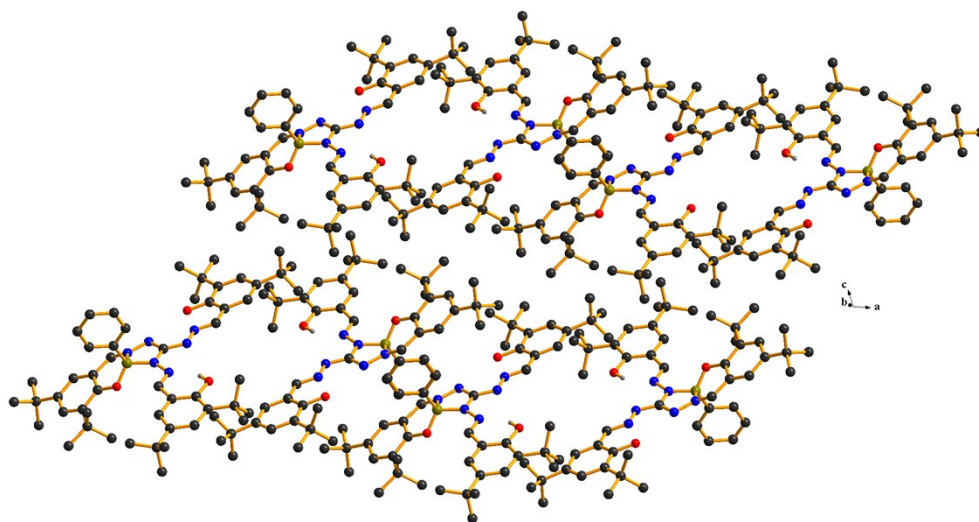


Fig. S23 Two-dimensional polymeric supramolecular network of **8**.

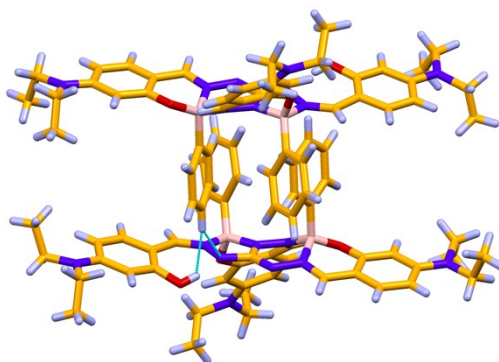


Fig. S24 Dimeric structure of compound **9**.

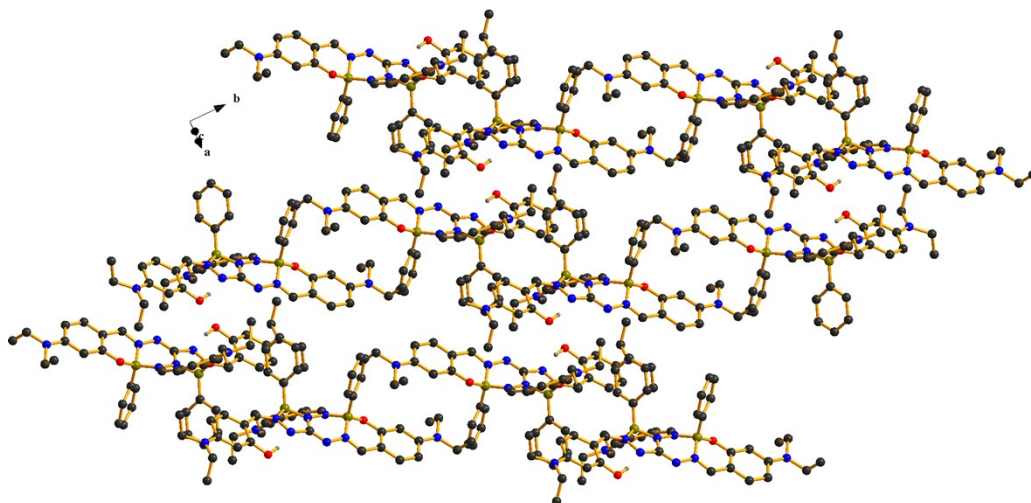


Fig. S25 Two-dimensional supramolecular network of **9**.

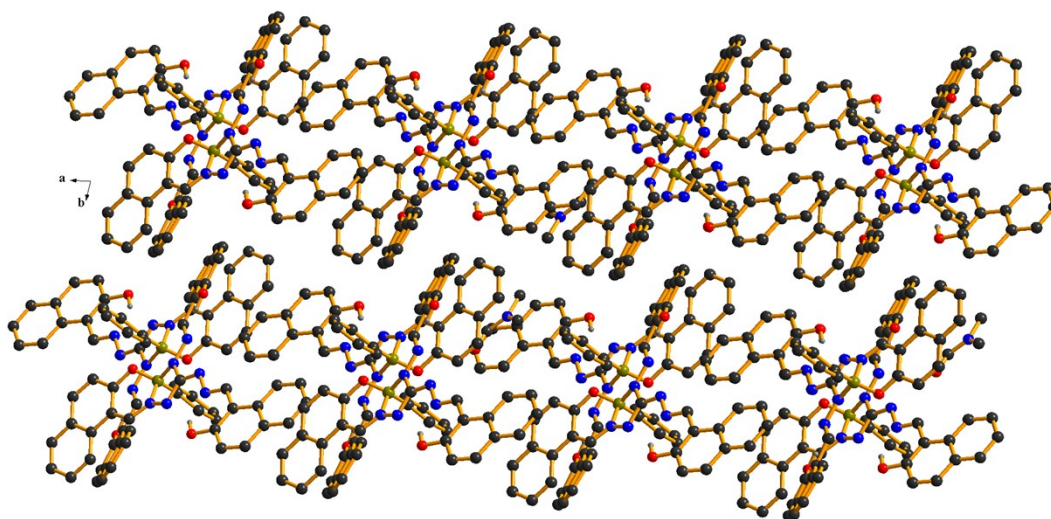


Fig. S26 Two-dimensional chain like supramolecular network of **10**.

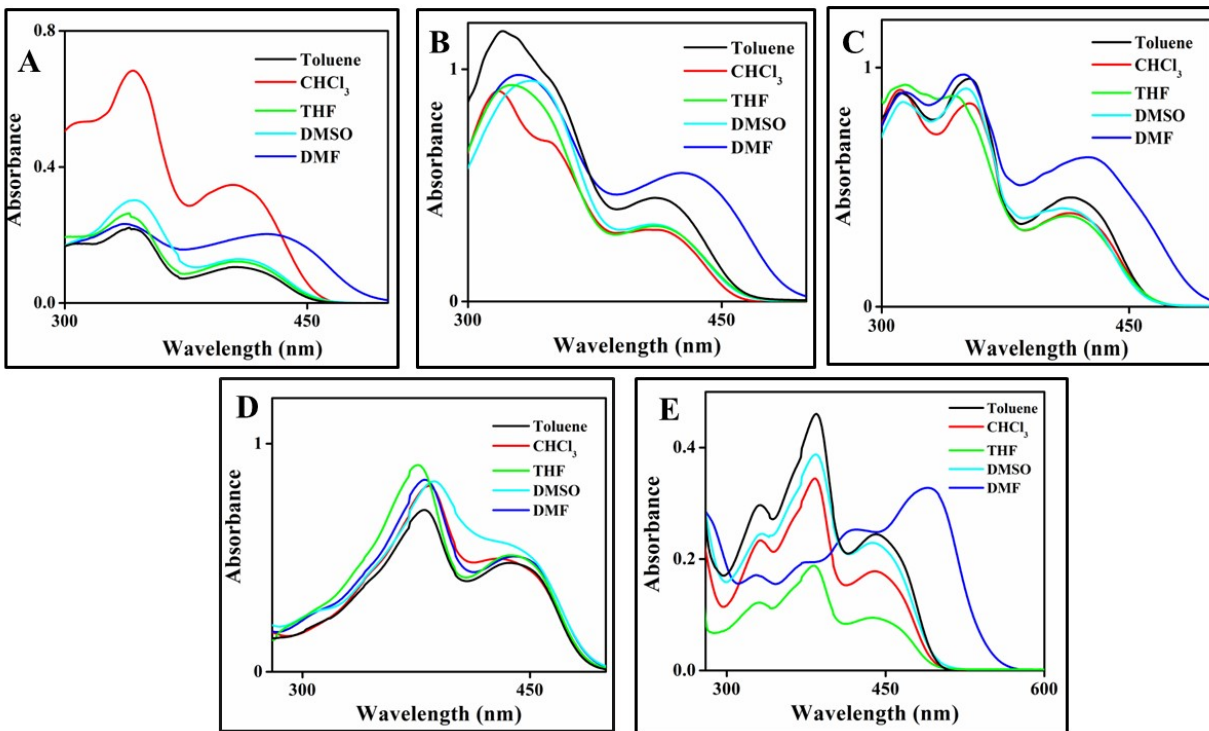


Fig. S27. Absorption spectra of boron compounds **6-10** (A - E) in various solvents with different polarities at room temperature.

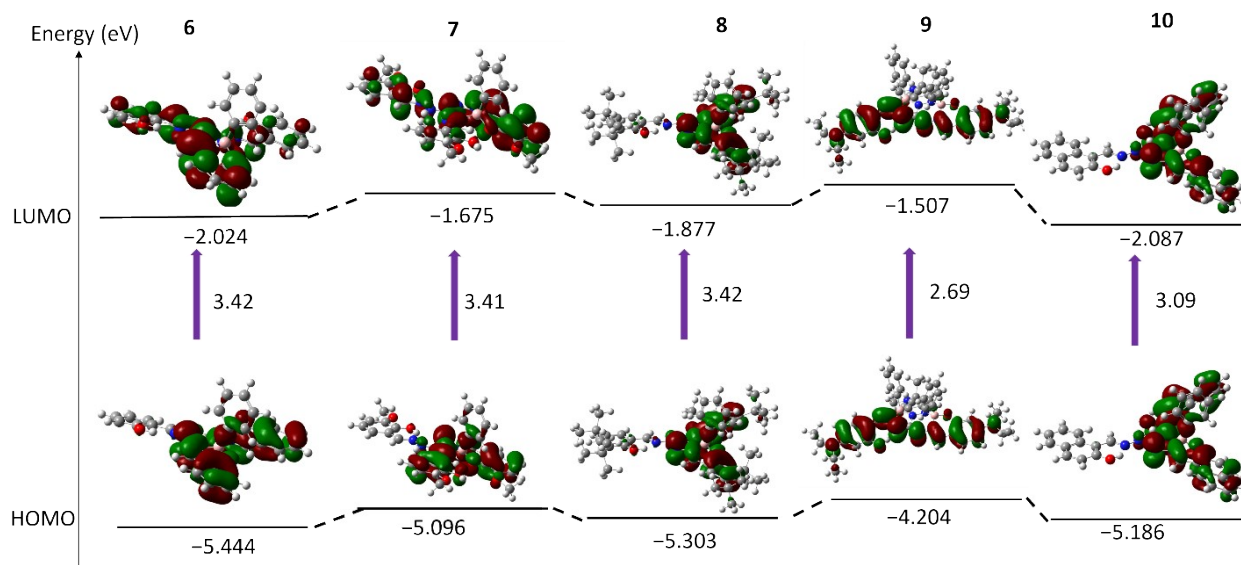


Fig. S28. Enol form of selected frontier molecular orbital of organoboron complexes **6-10** based on optimized ground state geometry. Calculation was performed at B3LYP/6-31G(d) level with Gaussian 16.

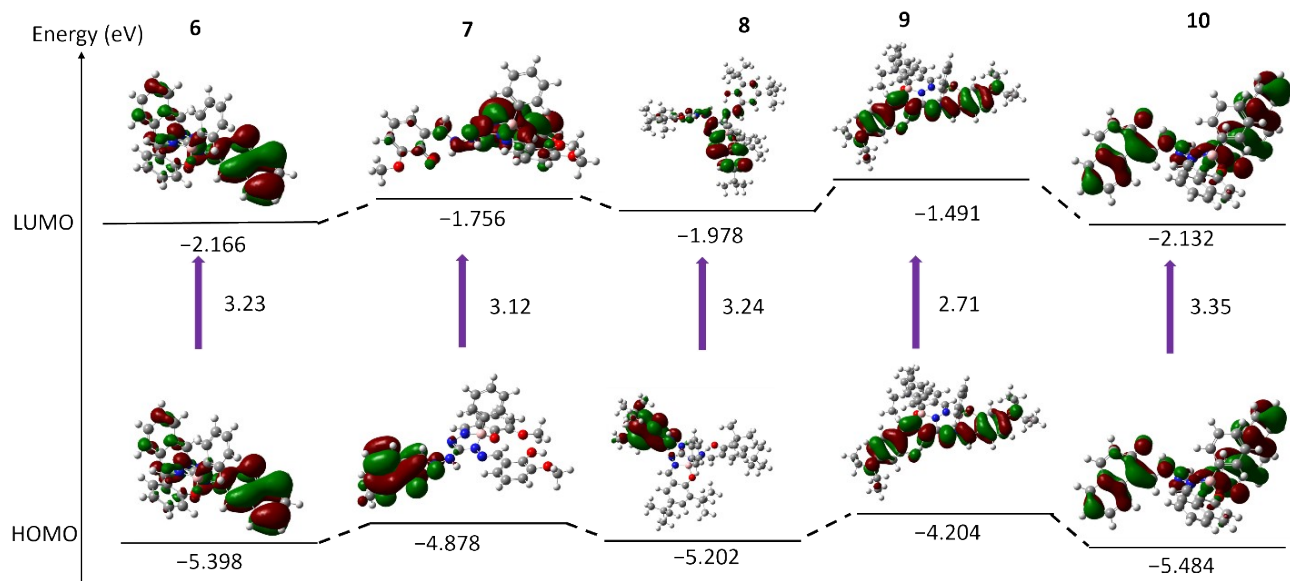


Fig. S29. Keto form of selected frontier molecular orbital of organoboron complexes **6-10** based on optimized ground state geometry. Calculation was performed at B3LYP/6-31G(d) level with Gaussian 16.

Table S2. Selected bond lengths (Å) for [6-10] from X-ray and calculated structures using the B3LYP 6-31G method.

	6	6 cal.	7	7 cal	8	8cal	9	9 cal	10	10cal
B1-N2	1.583(4)	1.582	1.574(2)	1.586	1.567(5)	1.578	1.520(3)	1.534	1.564(3)	1.574
B1-N3	1.566(4)	1.568	1.561(3)	1.566	1.542(3)	1.567	1.571(5)	1.593	1.561(1)	1.565
B1-O1	1.450(4)	1.468	1.459(3)	1.465	1.454(3)	1.469	1.462(4)	1.478	1.463(1)	1.472
B1-C23	1.597(3)	1.612	1.611(3)	1.566	1.605(5)	1.616	1.592(1)	1.593	1.607(2)	1.614
B1-N2							1.573(3)	1.587		
B1-N3							1.566(2)	1.579		
B1-O1							1.444(3)	1.462		
B1-C23							1.599(2)	1.612		

Table S3. Electronic transition for organoboron complexes 6-10 calculated using the B3LYP 6-31G method.

Complexes	Transition	MO Contribution	Energy gap		Oscillator Strength (f)
			ev	nm	
6	S ₀ -S ₁	HOMO → LUMO	3.42	371	0.4242
7	S ₀ -S ₁	HOMO → LUMO	3.41	377	0.3129
8	S ₀ -S ₁	HOMO → LUMO	3.42	374	0.3617
9	S ₀ -S ₁	HOMO → LUMO	2.69	416	0.4507
10	S ₀ -S ₁	HOMO → LUMO	3.09	400	0.5116

Table S4. UV-visible absorption and emission spectra of **6-10** in different solvents at room temperature.

Solvents		Toluene	CHCl₃	THF	DMSO	DMF
6	λ_{abs} (nm)	342, 409	343, 405	341, 409	342, 409	338, 432
	λ_{em} (nm)	485, 507	487, 505	485, 502	479, 518	481, 515
	Φ_{F}	0.006	0.010	0.001	0.016	0.020
7	λ_{abs} (nm)	320,414	317,415	327,415	338,415	330,428
	λ_{em} (nm)	500,535	499	510	496,544	498,463
	Φ_{F}	0.008	0.007	0.004	0.009	0.014
8	λ_{abs} (nm)	353, 416	354, 416	344, 415	352, 413	350, 428
	λ_{em} (nm)	482, 522	481, 499	480, 501	482, 518	478, 533
	Φ_{F}	0.016	0.017	0.006	0.004	0.040
9	λ_{abs} (nm)	379, 439	380, 436	376, 441	386, 443	382, 440
	λ_{em} (nm)	541	509, 560	503, 556	478,573	574
	Φ_{F}	0.012	0.046	0.005	0.012	0.088
10	λ_{abs} (nm)	330, 383, 441	331, 383, 441	329, 382, 441	332, 384, 437	329, 371, 492
	λ_{em} (nm)	507, 533	501, 529	503,530	507,539	550
	Φ_{F}	0.052	0.026	0.004	0.006	0.031

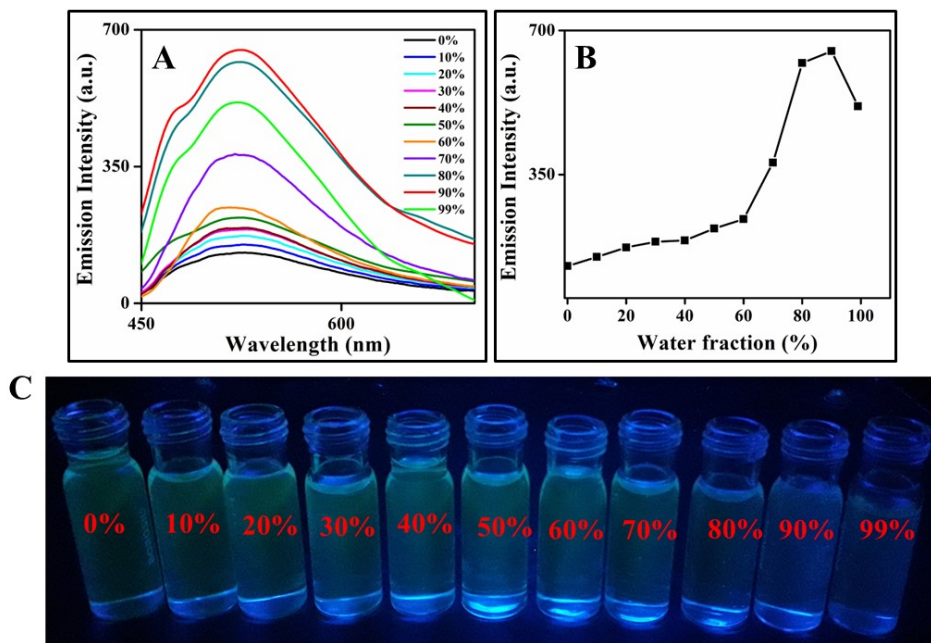


Fig. S30. (A) Emission spectra of **6** in different water fractions in THF and water mixture binary solvent; $\lambda_{\text{ex}} = 420$ nm. (B) Plots of emission intensity vs water fraction. (C) Fluorescent images in different water fractions (under UV light).

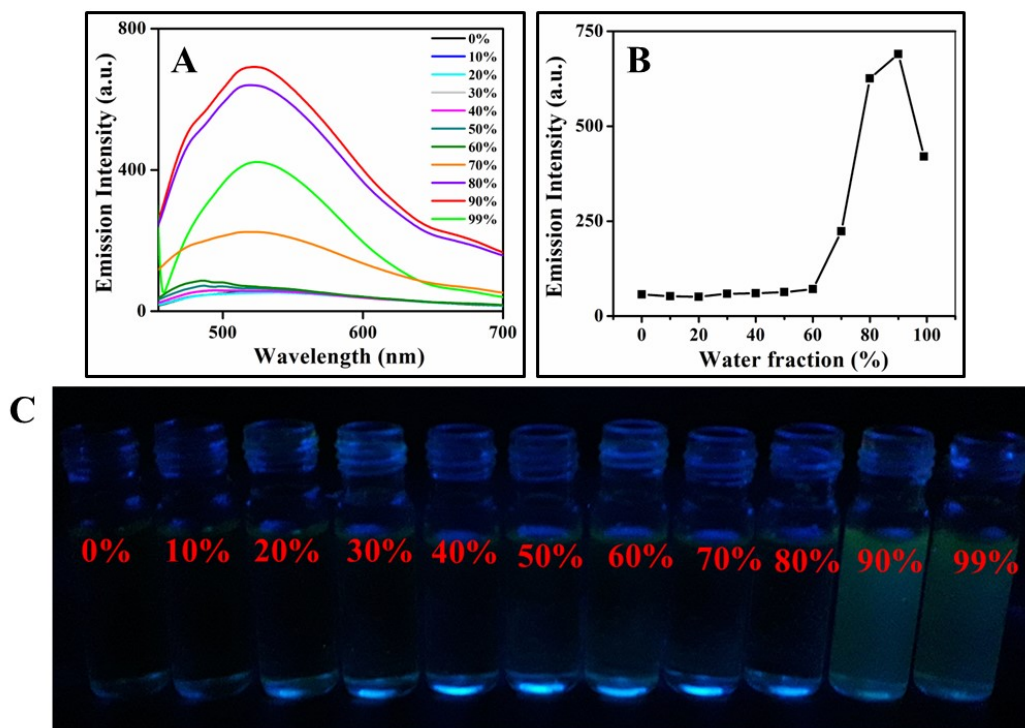


Fig. S31. (A) Emission spectra of **7** in different water fractions in THF and water mixture binary solvent; $\lambda_{\text{ex}} = 420$ nm. (B) Plots of emission intensity vs water fraction. (C) Fluorescent images of **7** in different water fractions (under UV light).

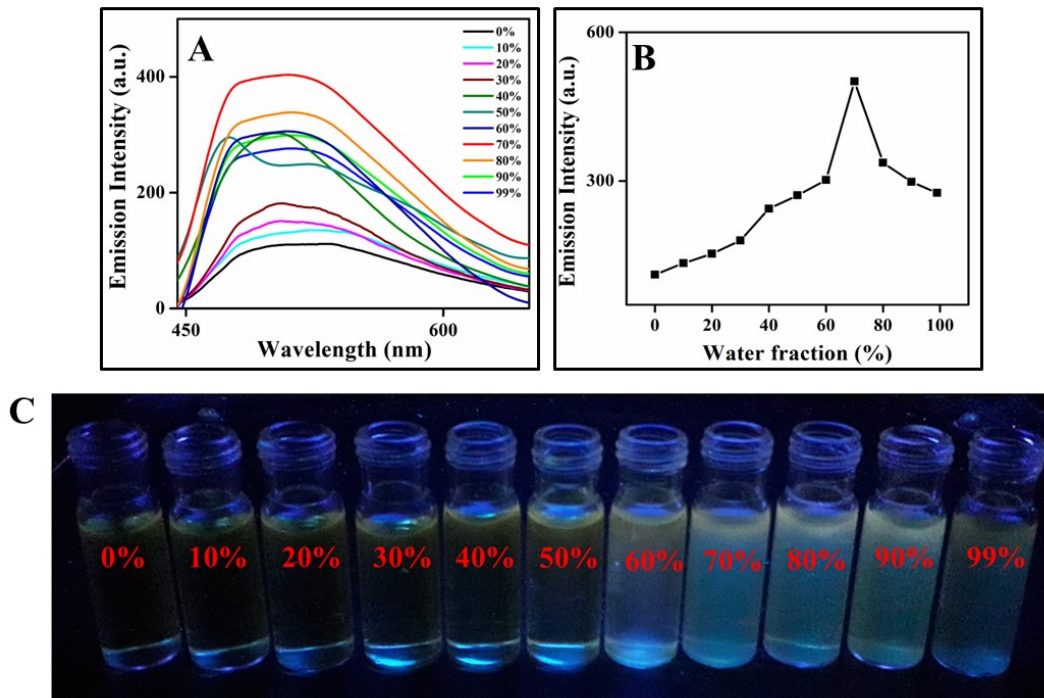


Fig. S32. (A) Emission spectra of **8** in different water fractions in THF and water mixture binary solvent; $\lambda_{\text{ex}} = 420$ nm. (B) Plots of emission intensity vs water fraction. (C) Fluorescent images of **8** in different water fractions (under UV light).

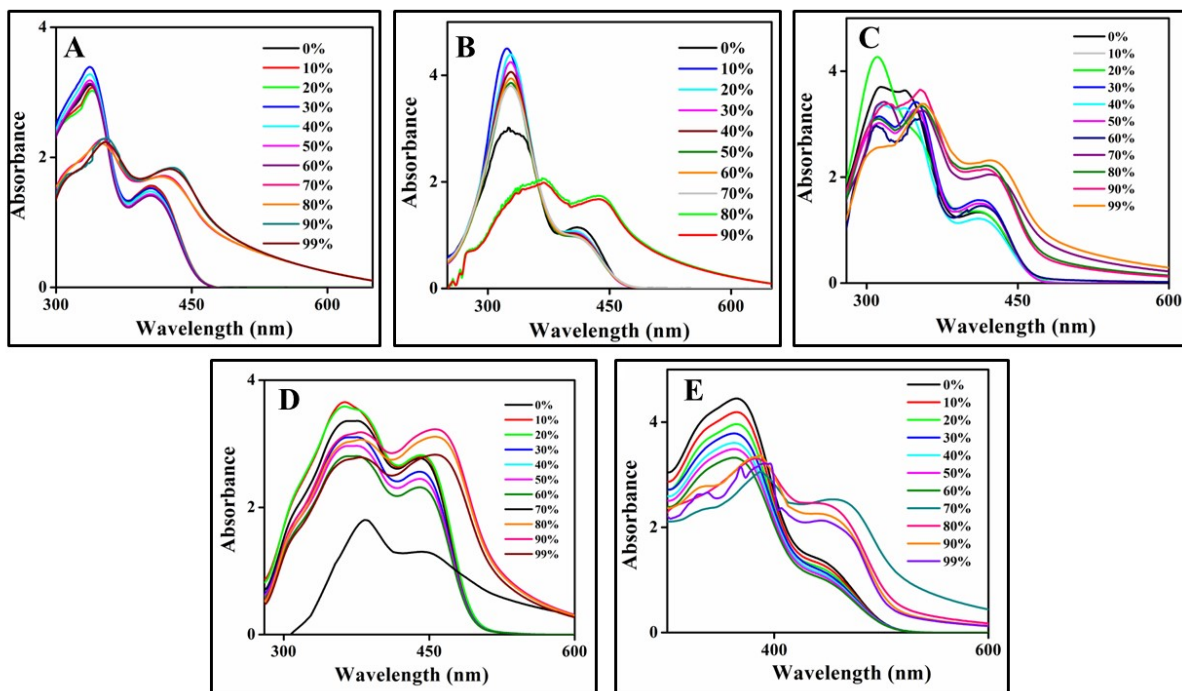


Fig. S33. UV-visible absorption spectra of compounds **6-10** (A-E) in THF-H₂O (0-90 %) mixture with different water fractions.

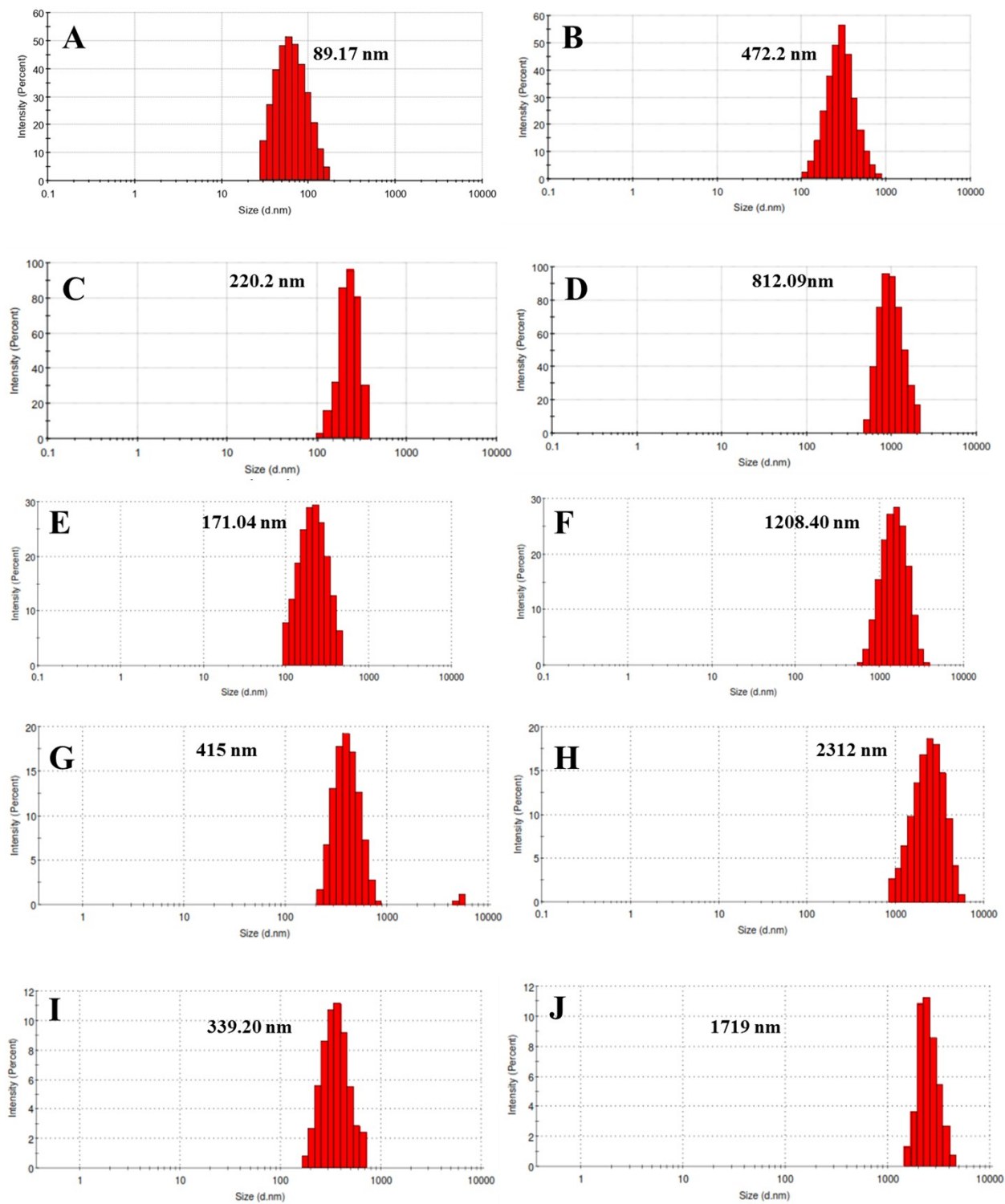


Fig. S34. DLS images of compounds (6-10) with particle size distribution in THF-H₂O mixture (A, B) **6** (60 & 90%), (C, D) **7** (70 & 90%), (E, F) **8** (50 & 70%), (G, H) **9** (70 & 90%) and (I, J) **10** (70 & 90%)

Table S5. Results from DLS for the complex **6-10**.

Complex	Percentage of water (%)	Particle size (nm)
6	60 & 90	89.17 & 472.2
7	70 & 90	220.2 & 812.09
8	50 & 70	171.04 & 1208.04
9	70 & 90	415 & 2312
10	70 & 90	339.20 & 1719

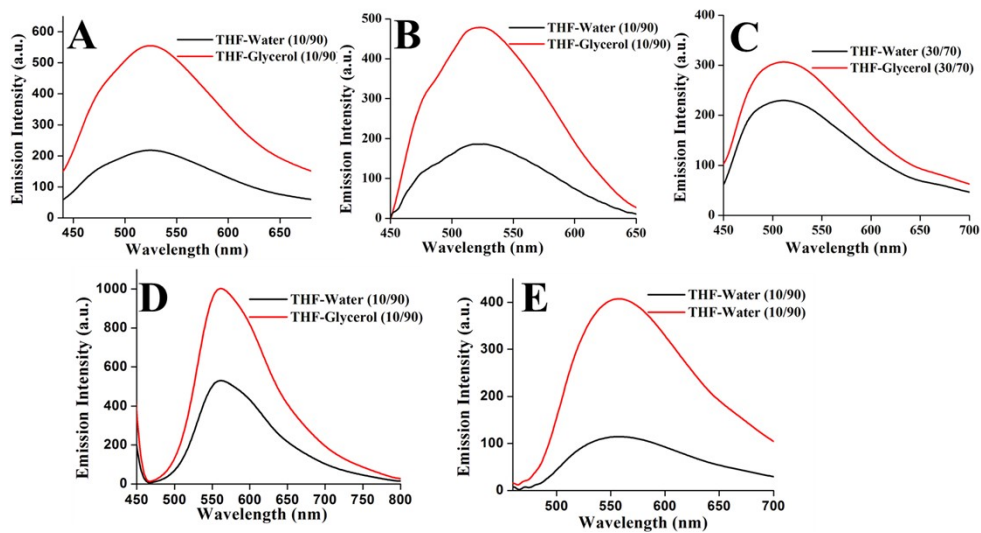


Fig. S35. Emission spectra of **6-10** in THF-H₂O and THF-glycerol.

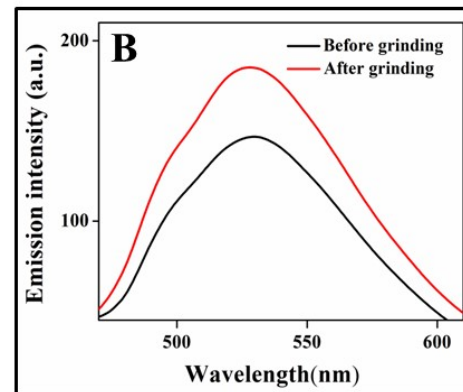
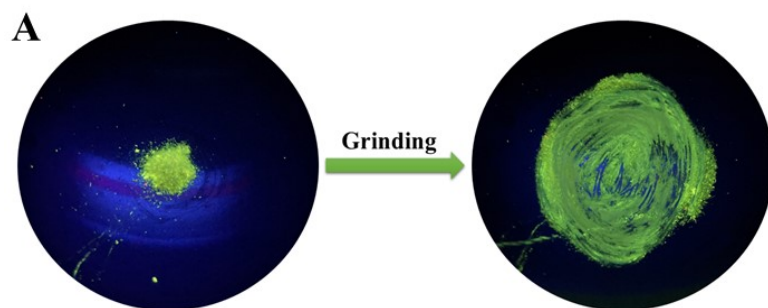
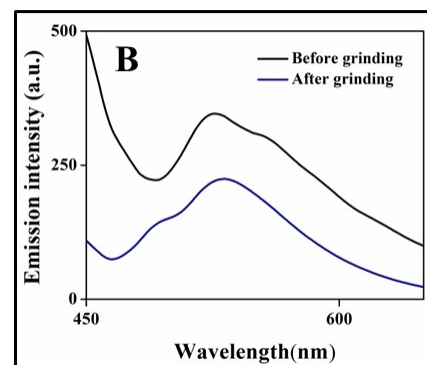
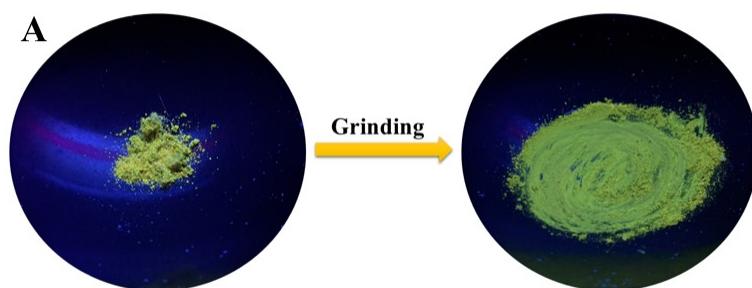


Fig. S36. (A). Images of the boron compounds (**7 & 8**) under UV-lamp. (B) Solid state emission spectra of compounds (**7 & 8**) crystals and ground samples.

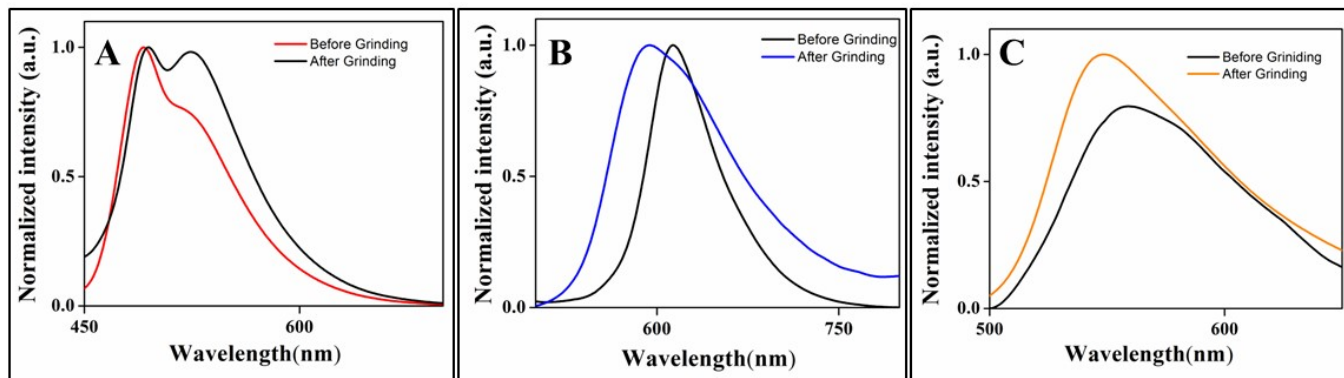


Fig. S37. (A) Normalized spectrum of the compound **6** before and after grinding. (B) Normalized spectrum of the compound **9** before and after grinding. (C) Normalized spectrum of the compound **10** before and after grinding.

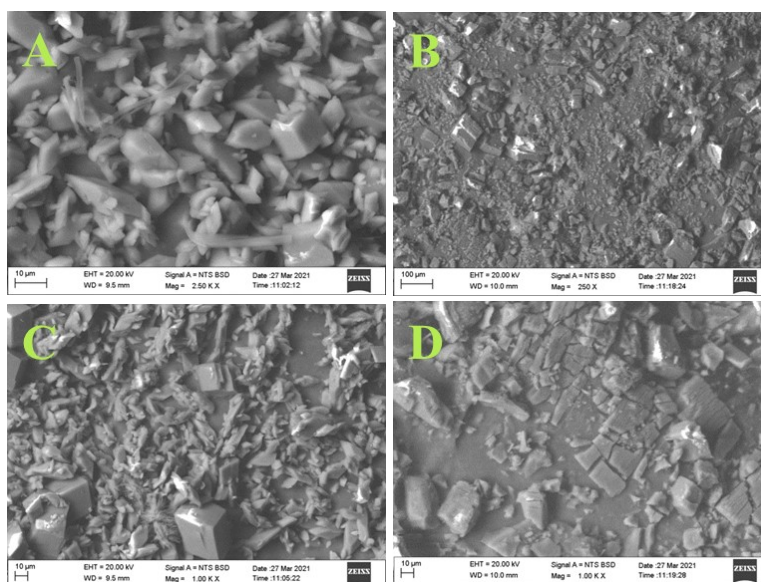


Fig. S38. SEM images of compounds **9** & **10** (A&B) before and (C&D) after grinding respectively.

Table S6. Crystal parameters and structure refinement data for compound **6-10**.

Parameters	6	7	8
Empirical formula	C ₂₈ H ₂₅ BN ₆ O ₄	C ₃₁ H ₂₉ BN ₆ O ₆ ·2(C ₂ H ₃ N),H ₂ O	C ₅₅ H ₇₅ B N _{7.50} O ₃
Formula weight	520.35	692.53	900.53
Temperature	100(2) K	295(2) K	100(2) K
Wavelength	0.71073 Å	0.71073 Å	0.71073 Å
Crystal system	Triclinic	Monoclinic	Triclinic
Space group	P-1	P2 ₁ /c	P-1
Unit cell dimensions	a = 9.9278(5) Å b = 14.8243(8) Å c = 17.6465(10) Å α = 104.209(3)° β = 91.481(3)° γ = 94.206(3)°	a = 12.1862(5) Å b = 28.1636(12) Å c = 10.6937(5) Å α = 90° β = 107.529(4)° γ = 90°	a = 14.3032(13) Å b = 14.3886(14) Å c = 14.4404(14) Å α = 93.878° β = 113.614(4)° γ = 90.966(5)°
Volume	2508.3(2) Å ³	3499.7(3) Å ³	2713.6(5) Å ³
Z	4	4	2
Density (calculated)	1.378 Mg/m ³	1.314 Mg/m ³	1.102 Mg/m ³
Absorption coefficient	0.094 mm ⁻¹	0.093 mm ⁻¹	0.069 mm ⁻¹
F(000)	1088	1456	974
Crystal size (mm ³)	0.45 x 0.30 x 0.080	0.32 x 0.12 x 0.09	0.45 x 0.20 x 0.17
Theta range for data collection	1.613 to 28.359°	3.75 to 28.75°	1.420 to 26.455°
Index ranges	-13<=h<=13, -19<=k<=19, -23<=l<=23	-16<=h<=12, -28<=k<=38, -10<=l<=14	-17<=h<=16, -17<=k<=17, -14<=l<=18
Reflections collected	21795	19478	15200
Independent reflections	21795[R(int) = 0.0572]	8402[R(int) = 0.0596]	10400 [R(int) = 0.0513]
Completeness to theta = 25.000°	99.3 %	96.7 %	94.3 %
Data / restraints / parameters	21795/7/727	8402/1/485	10400 / 105 / 672
Goodness-of-fit on F ²	1.024	1.026	1.013
Final R indices [I>2σ(I)]	R1 = 0.0650, wR2 = 0.1467	R1 = 0.0596, wR2 = 0.10896	R1 = 0.0704, wR2 = 0.1644
R indices (all data)	R1 = 0.1012, wR2 = 0.1665	R1 = 0.1089, wR2 = 0.1445	R1 = 0.1448, wR2 = 0.2010
Largest diff. peak and hole (e.Å ⁻³)	1.550, -0.462	0.194, -0.216	0.448, -0.283

Parameters	9	10
Empirical formula	C ₄₆ H ₅₃ B ₂ N ₉ O ₃	C ₄₃ H ₃₆ BN ₇ O ₄
Formula weight	801.59	725.60
Temperature	100(2) K	100(2)K
Wavelength	0.71073 Å	0.71073
Crystal system	Triclinic	Triclinic
Space group	P-1	P-1
Unit cell dimensions	a = 13.9824(9) Å b = 19.1267(12) Å c = 20.5066(13) Å α = 90.406(4)° β = 108.715(3)° γ = 90.449(3)°	a = 11.3918(7) Å b = 11.9970 (8) Å c = 13.9478 (8) Å α = 75.157(3)° β = 89.324(3)° γ = 79.110(4)°
Volume	5193.8(6) Å ³	1808.1(2) Å ³
Z	4	2
Density (calculated)	1.025Mg/m ³	1.333 Mg/m ³
Absorption coefficient	0.065 mm ⁻¹	0.087 mm ⁻¹
F(000)	1704	760
Crystal size (mm ³)	0.29 x 0.15 x 0.10	0.30 x 0.12 x 0.07
Theta range for data collection	1.487 to 25.027°	1.511 to 28.399°
Index ranges	-16<=h<=16, -22<=k<=22, -24<=l<=24	-15<=h<=15, -16<=k<=15, -18<=l<=18
Reflections collected	36644	17847
Independent reflections	18339[R(int) = 0.0348]	8985 [R(int) = 0.0361]
Completeness to theta = 25.000°	99.8 %	100.0 %
Data / restraints / parameters	18339 / 115 / 1096	8985 / 0 / 505
Goodness-of-fit on F ²	1.047	1.030
Final R indices [I>2sigma(I)]	R1 = 0.0682, wR2 = 0.1870	R1 = 0.0424, wR2 = 0.0989
R indices (all data)	R1 = 0.1011, wR2 = 0.2119	R1 = 0.0675, wR2 = 0.1133
Largest diff. peak and hole (eÅ ⁻³)	0.688, -0.404	0.314, -0.251

Reference

1. M. J. Frisch, G. W. Trucks, H. B. Schlegel, G. E. Scuseria, M. A. Robb, J. R. Cheeseman, G. Scalmani, V. Barone, G. A. Petersson, H. Nakatsuji, Gaussian 16, Rev. C. 01, Gaussian, Inc., Wallingford, CT. 2016.
2. J. Jia and J. Wen, *Tetrahedron Lett.*, 2021, **71**, 153006.
3. H. Wang, X. Guo, W. Bu, Z. Kang, C. Yu, Q. Wu, L. Jiao and E. Hao, *Dyes Pigm.*, 2023, **210**, 111013.
4. M. M. Alcaide, F. M. Santos, V. n. F. Pais, J. I. s. Carvalho, D. Collado, E. Pérez-Inestrosa, J. s. F. Arteaga, F. Boscá, P. M. Gois and U. Pischel, *J. Org. Chem.*, 2017, **82**, 7151-7158.
5. F. M. Santos, Z. Domínguez, J. P. Fernandes, C. Parente Carvalho, D. Collado, E. Pérez-Inestrosa, M. V. Pinto, A. Fernandes, J. F. Arteaga and U. Pischel, *Chem. Eur. J.*, 2020, **26**, 14064-14069.
6. C. Yu, G. Di, Q. Li, X. Guo, L. Wang, Q. Gong, Y. Wei, Q. Zhao, L. Jiao and E. Hao, *Inorg. Chem.*, 2024, **63**, 21397-21409.